

1 **Toward consistency between trends in bottom-up CO<sub>2</sub>**  
2 **emissions and top-down atmospheric measurements in**  
3 **the Los Angeles megacity**

4 **S. Newman<sup>1</sup>, X. Xu<sup>2</sup>, K. R. Gurney<sup>3</sup>, Y.-K. Hsu<sup>4</sup>, K.-F. Li<sup>5</sup>, X. Jiang<sup>6</sup>, R.**  
5 **Keeling<sup>7</sup>, S. Feng<sup>8,\*</sup>, D. O'Keefe<sup>3</sup>, R. Patarasuk<sup>3</sup>, K. W. Wong<sup>8</sup>, P. Rao<sup>8</sup>, M. L.**  
6 **Fischer<sup>9</sup>, and Y. L. Yung<sup>1</sup>**

- 7  
8  
9 [1]{Division of Geological and Planetary Sciences, California Institute of Technology,  
10 Pasadena, CA 91125, USA}  
11 [2]{Department of Earth System Science, University of California, Irvine, CA 92697,  
12 USA}  
13 [3]{School of Life Sciences, Arizona State University, Tempe, AZ 85287, USA}  
14 [4]{Monitoring and Laboratory Division, Air Resources Board, Sacramento, CA 95811,  
15 USA}  
16 [5]{Department of Applied Mathematics, University of Washington, Seattle, WA 98195,  
17 USA}  
18 [6]{Department of Earth and Atmospheric Sciences, University of Houston, Houston, TX  
19 77004, USA}  
20 [7]{Scripps Institution of Oceanography, University of California, San Diego, La Jolla,  
21 CA 92037, USA}  
22 [8]{Earth Atmospheric Science, Jet Propulsion Laboratory, California Institute of  
23 Technology, Pasadena, CA 91109}  
24 [9]{Environmental Energy Area, E. O. Lawrence Berkeley National Laboratory,  
25 Berkeley, CA 94720, USA}  
  
26 [\*]{now at Department of Meteorology, Pennsylvania State University, University Park,  
27 PA 16802, USA}

Sally Newman 2/18/2016 11:30 PM  
Deleted: trends

28  
29  
30  
31

33 **Abstract**

34 Large urban emissions of greenhouse gases result in large atmospheric  
35 enhancements relative to background that are easily measured. Using CO<sub>2</sub> mole fractions  
36 and Δ<sup>14</sup>C and δ<sup>13</sup>C values of CO<sub>2</sub> in the Los Angeles megacity observed in inland  
37 Pasadena (2006-2013) and coastal Palos Verdes peninsula (autumn 2009-2013), we have  
38 determined time series for CO<sub>2</sub> contributions from fossil fuel combustion (C<sub>ff</sub>) for both  
39 sites and broken those down into contributions from petroleum/gasoline and natural gas  
40 burning for Pasadena. We find a 10 % reduction in Pasadena C<sub>ff</sub> during the Great  
41 Recession of 2008-2010, which is consistent with the bottom-up inventory determined by  
42 the California Air Resources Board. The isotopic variations and total atmospheric CO<sub>2</sub>  
43 from our observations are used to infer seasonality of natural gas and petroleum  
44 combustion. The trend of CO<sub>2</sub> contributions to the atmosphere from natural gas  
45 combustion is out of phase with the seasonal cycle of total natural gas combustion  
46 seasonal patterns in bottom-up inventories but is consistent with the seasonality of natural  
47 gas usage by the area's electricity generating power plants. For petroleum, the inferred  
48 seasonality of CO<sub>2</sub> contributions from burning petroleum is delayed by several months  
49 relative to usage indicated by statewide gasoline taxes. Using the high-resolution Hestia-  
50 LA data product to compare C<sub>ff</sub> from parts of the basin sampled by winds at different  
51 times of year, we find that variations in observed fossil fuel CO<sub>2</sub> reflect seasonal  
52 variations in wind direction. The seasonality of the local CO<sub>2</sub> excess from fossil fuel  
53 combustion along the coast, on Palos Verdes peninsula, is higher in fall and winter than  
54 spring and summer, almost completely out of phase with that from Pasadena, also  
55 because of the annual variations of winds in the region. Variations in fossil fuel CO<sub>2</sub>

Sally Newman 2/18/2016 11:36 PM  
**Deleted:** For natural gas, inferred emissions

Sally Newman 2/18/2016 11:37 PM  
**Deleted:** are

Sally Newman 2/18/2016 11:37 PM  
**Deleted:** are

Sally Newman 2/18/2016 11:37 PM  
**Deleted:** emissions

Sally Newman 2/19/2016 5:32 PM  
**Deleted:** emissions

61 signals are consistent with sampling the bottom-up Hestia-LA fossil CO<sub>2</sub> emissions  
62 product for sub-city source regions in the LA megacity domain when wind directions are  
63 considered.  
64

65 **1 Introduction**

66 Carbon dioxide is the most important greenhouse gas (GHG) contributing to  
67 current global warming, contributing 64 % of the total radiative forcing, according to the  
68 IPCC AR5 report (IPCC, 2013) and comprising 82 % of GHG emissions (NRC, 2010).  
69 The global average mole fraction of CO<sub>2</sub> has increased approximately 40 % since pre-  
70 industrial times due to anthropogenic emissions (IPCC, 2013). Since the proportion of  
71 the world’s emissions from megacities (urban regions with more than 10 million  
72 inhabitants) is out of proportion with their small surface area (EDGAR, 2009; IEA,  
73 2008), quantifying C<sub>fr</sub> is essential if we are to work aggressively toward their reduction  
74 (Duren and Miller, 2012). As a consequence of global warming mitigation, reducing C<sub>fr</sub>  
75 could reduce air pollution mortality, which is correlated with increased CO<sub>2</sub> levels  
76 (Jacobson, 2008).

77 Identifying the sources of emissions is a major first step in understanding and  
78 mitigating anthropogenic contributions. In cities, especially in megacities, these CO<sub>2</sub>  
79 sources often dominate over the normally predominant natural source of the biosphere, at  
80 least during certain seasons (e.g., Pataki et al., 2003; Widory and Javoy, 2003; Newman  
81 et al., 2013; 2008; Lopez et al., 2013; Turnbull et al., 2011; 2015; Vardag et al., 2015).  
82 The most common method of inventorying CO<sub>2</sub> emissions from human activities is  
83 through bottom-up reporting by governmental agencies, following IPCC methods (IPCC,  
84 2013). Uncertainties in these methods range from 3-5 % to greater than 50 % (Andres et  
85 al., 2012). A more recent, scientifically-based bottom-up approach has been pioneered  
86 through the Vulcan and Hestia projects (Gurney et al., 2009; Gurney et al., 2012). These  
87 efforts combine multiple streams of data such as air pollution reporting, demographics,

Sally Newman 2/19/2016 5:32 PM

**Deleted:** these emissions

Sally Newman 2/19/2016 5:33 PM

**Deleted:** CO<sub>2</sub> emissions

Sally Newman 2/18/2016 11:38 PM

**Deleted:** This requires self-reporting and may not be reliable in some parts of the world.

92 property tax data, and traffic monitoring, to arrive at what is proving to be a much more  
93 accurate and space/time detailed estimate of fossil fuel CO<sub>2</sub> emissions. The Vulcan  
94 Project accomplished fossil fuel CO<sub>2</sub> emission estimation for the whole US at spatial  
95 scales of 10 km every hour of the year 2002, with updated years expected by the end of  
96 2015. Hestia is specifically focused on the urban domain and has accomplished  
97 estimation down to the individual building and street segment scale for four cities  
98 (Indianapolis, IN; Salt Lake City, UT; Los Angeles basin, CA; Phoenix, AZ) with work  
99 ongoing in Baltimore, MD (Gurney et al., 2012, Patarasuk et al., in prep.; Rao et al.,  
100 2015). Both of these detailed data products are available for selected cities in the United  
101 States, facilitating top-down emissions quantification through long-term ambient air  
102 monitoring (Duren and Miller, 2012; Gurney et al., 2015). Trends in  $C_{ff}$  must be  
103 monitored precisely in order to evaluate progress towards mandated emission reductions.  
104 As an example, the California Global Warming Solutions Act of 2006 (Assembly Bill 32)  
105 requires reduction of greenhouse gas emissions to 1990 levels by 2020, a reduction of  
106 about 15 %. Indeed, now is the time to document the current level of emissions, as  
107 governments begin to implement strategies to reduce emissions (e.g., California's Cap-  
108 and-Trade Program and Low Carbon Fuel Standards) and want to be able to assess their  
109 efficacy.

110 Within megacities, atmospheric CO<sub>2</sub> concentrations are often highly elevated  
111 relative to the regional background due to locally emitted carbon dioxide. This excess  
112 can be analyzed for its isotopic composition to help attribute the local emissions to  
113 specific processes. Radiocarbon (<sup>14</sup>C) analyses give quantitative information as to the  
114 proportions of CO<sub>2</sub> resulting from combustion of ancient sources of carbon (fossil fuels)

Sally Newman 2/19/2016 5:33 PM

Deleted: CO<sub>2</sub> emissions

116 relative to sources incorporating modern carbon, such as the biosphere (e.g., Levin et al.,  
117 2003; Levin and Roedenbeck, 2008; Turnbull et al., 2009), because of its short half-life  
118 of 5730 years. The stable isotopes of carbon can be used to separate sources with  
119 differing values, such as natural gas and petroleum combustion, with the  $^{13}\text{C}/^{12}\text{C}$  ratio of  
120 natural gas typically being lower than that of petroleum (e.g., Keeling, 1961; 1958;  
121 Newman et al., 2008; 2013; Pataki et al., 2003; Widory and Javoy, 2003; Djuricin et al.,  
122 2010; Moore and Jacobson, 2015), although there can be overlap between petroleum  
123 combustion and biological respiration. Therefore, if we know the biosphere's  
124 contribution from the fossil fuel  $\text{CO}_2$  contribution derived from  $\Delta^{14}\text{C}$  and the total  $\text{CO}_2$   
125 enhancement over background, we can distinguish all three sources (biosphere, petroleum  
126 combustion, and natural gas combustion) provided that there are large variations, such as  
127 in urban regions.

128 Here we report the use of  $^{14}\text{C}$  combined with  $\delta^{13}\text{C}$  in flask samples to disaggregate  
129 the local emissions of  $\text{CO}_2$  in the Los Angeles (LA) basin into biosphere, natural gas, and  
130 petroleum combustion sources. We investigate the annual patterns and trends for 2006-  
131 2013 in these components and compare them to global background and to bottom-up  
132 inventories generated by government agencies and scientific colleagues. In particular, we  
133 test the method against the changes in  $\text{C}_{\text{ff}}$  observed during and after the Great Recession  
134 of 2008-2010 in LA.

135 The sampling, analytical methods, and calculations are described in section 2.  
136 Section 3 discusses the results with regard to spatial and temporal variations and  
137 comparison with bottom-up inventories and the detailed data product Hestia-LA. Overall  
138 conclusions are presented in section 4.

Sally Newman 2/19/2016 5:34 PM  
Deleted: emissions

140

## 141 **2 Data and analysis**

### 142 **2.1 Locations**

143 Samples were collected at two locations in the Los Angeles basin: on the campus  
144 of the California Institute of Technology (Caltech) in Pasadena, CA (34°8'12"N,  
145 118°7'39"W, (240 ± 5) m above sea level), and on Palos Verdes peninsula overlooking  
146 the Pacific Ocean and Santa Catalina Island to the south (33°44.7'N, 118°20.9'W, 330 m  
147 above sea level) (Fig.1). Pasadena is located in the San Gabriel valley, approximately 14  
148 km NE of downtown Los Angeles and 40 km from the coast. Prevailing winds from the  
149 SW bring marine air from the ocean during daytime hours, as the planetary boundary  
150 layer deepens during heating of the land. During these periods of prevailing south to  
151 west winds, the Palos Verdes site is a credible background site. Since the marine air  
152 picks up emissions from the basin during its transit inland, Pasadena is a good receptor  
153 site for LA emissions. The San Gabriel Mountains just 5 km to the north act as a barrier  
154 until midday, when upslope flow and the rising temperature inversion layer allow venting  
155 over the mountains (Lu and Turco, 1994; 1995).

156

### 157 **2.2 Samples**

158 Air samples were collected into evacuated one-liter Pyrex flasks through Synflex  
159 1300 tubing after passing through  $Mg(ClO_4)_2$  to dry the samples. In Pasadena, samples  
160 were collected on alternate afternoons at 1400 Pacific Standard Time (PST) using an  
161 autosampler, whereas at the Palos Verdes site samples were collected manually once a  
162 week (on weekend days) between 1100 and 1600 PST, and typically near 1400 PST. The

163 mid-afternoon sampling time was chosen because this is when the planetary boundary  
164 layer tends to be the deepest and most well mixed during the day. The sampling path at  
165 each location was purged with ambient air before collection.

166 CO<sub>2</sub> was extracted from the air samples cryogenically, following the methods described  
167 in Newman et al. (2008), with the amount of CO<sub>2</sub> determined manometrically. Then the  
168  $\delta^{13}\text{C}$  was determined relative to the Vienna PDB (VPDB) standard (Coplen, 1996) by  
169 dual-inlet isotope ratio mass spectrometry (Thermo-Finnigan MAT 252; Bremen,  
170 Germany) on each individual sample. After this analysis, the CO<sub>2</sub> was frozen into a cold  
171 finger and combined with 3-7 other individual samples to create a composite sample  
172 characterizing mid-afternoon air over a two-week (Pasadena) or month (Palos Verdes)  
173 time period for  $\Delta^{14}\text{C}$  analysis. This differs from the sampling protocol of Affek et al.  
174 (2006), who collected on average two 5-liter samples per month, analyzed each sample  
175 separately, and then averaged the results to produce monthly average  $\Delta^{14}\text{C}$  values for  
176 2004-2005. We found that by combining smaller samples collected more frequently  
177 (alternate days in Pasadena) our results were less scattered than in the previous report and  
178 therefore give interpretable seasonal variations.  $\Delta^{14}\text{C}$  was analyzed by accelerator mass  
179 spectrometer at the Keck-CCAMS facility at the University of California, Irvine, using  
180 the methods described in Newman et al. (2013) and Xu et al. (2007). Analyses of air  
181 from standard tanks calibrated by NOAA (National Oceanic and Atmospheric  
182 Administration) gave errors for CO<sub>2</sub> mole fractions averaging of  $\pm 1.4$  ppm (1 ppm = 1  
183  $\mu\text{mol mol}^{-1}$ ) (n = 44) and  $\delta^{13}\text{C}$  of  $\pm 0.15$  ‰ (n = 30), including extraction, manometry,  
184 and mass spectrometry. Although the uncertainties in the CO<sub>2</sub> mole fractions is much  
185 higher than by spectroscopic techniques, it contributes less than half of the total

Sally Newman 2/22/2016 12:30 PM

**Deleted:** Pee Dee Belemnite (

Sally Newman 2/22/2016 12:30 PM

**Deleted:** )

Sally Newman 2/22/2016 12:57 PM

**Deleted:** Gonfiantini

Sally Newman 2/22/2016 12:58 PM

**Deleted:** 1978

Sally Newman 2/19/2016 5:34 PM

**Deleted:** CCMAS



191 | uncertainty in  $C_{ff}$ , which is dominated by the  $\Delta^{14}C$  average error of 2 ‰, based on long-  
192 | term reproducibility of secondary standards (Xu et al., 2007; Xu et al., 2010; Graven et  
193 | al, 2013; Miller et al., 2013).

194

## 195 | **2.3 Calculations**

196 | A major goal of this study is the attribution of the sources of the  $C_{ff}$  observed. A  
197 | schematic figure of the flow of data used to calculate the portion of the total  $CO_2$  that is  
198 | due to biosphere respiration (bio) and fossil fuel (ff) combustion, including burning of  
199 | petroleum (pet) and natural gas (ng), is shown in Fig. 2. Mole fractions of  $CO_2$  measured  
200 | at the two sites and a background site in La Jolla, CA, were used to calculate the  $CO_2$   
201 | excess (xs) over background (bg). The contributions of fossil fuel combustion and the  
202 | biosphere to the excess were determined from radiocarbon measurements, and the fossil  
203 | fuel component was further broken down into petroleum and natural gas using  $\delta^{13}C$  of the  
204 |  $CO_2$ . Details are described below.

205

### 206 | **2.3.1 Total $CO_2$ emissions and background $CO_2$ mole fraction**

207 | The  $CO_2$  excess caused by local emissions at the two sites was calculated by  
208 | subtracting an estimate of the background  $CO_2$  mole fraction derived from La Jolla  
209 | monthly values (Keeling et al., 2005; Figs. 3 and 4). Flask sampling at La Jolla is done  
210 | so as to minimize the influence of local  $CO_2$  sources by sampling during periods that  
211 | simultaneously satisfy three criteria: low variability in  $CO_2$  concentration for periods of  
212 | 3 hours or more, wind speed of  $2.6 \text{ m s}^{-1}$  or more from a narrow southwesterly to  
213 | westerly sector, and high visibility. That these methods successfully minimize influences

Sally Newman 2/19/2016 5:35 PM

Deleted:  $CO_2$  emissions

215 of local fossil-fuel emissions is indicated by the consistency of the annual radiocarbon  
 216 concentrations at La Jolla compared to clean stations both to the north and south in the  
 217 Northern Hemisphere (Graven, 2012). In this paper, therefore, the La Jolla data  
 218 presented are screened background data. The La Jolla data were interpolated to  
 219 determine the appropriate value for the midpoint of the range of collection dates included  
 220 in each  $\Delta^{14}\text{C}$  sample, using the algorithm from Thoning et al. (1989), with two harmonic  
 221 terms, three polynomial terms, and the smoothed residuals of the long term trend (cutoff  
 222 of 667 days).

223

### 224 **2.3.2 CO<sub>2</sub> from fossil fuels, based on $\Delta^{14}\text{C}$**

225 Mass balance calculations were used to calculate the relative contributions of  
 226 background air, biosphere respiration and photosynthesis, and fossil fuel combustion  
 227 (including natural gas and oil) to the CO<sub>2</sub> collected at the two sites. The following  
 228 equations quantitatively separate the background air, biosphere, and fossil fuel  
 229 combustion contributions to the locally measured atmospheric CO<sub>2</sub> using  $\Delta^{14}\text{C}$  (e.g.,  
 230 Levin et al., 2003; Miller et al., 2012; Pataki et al., 2003; Turnbull et al., 2006; Fig. 4):

$$231 \quad C_{\text{obs}} = C_{\text{bg}} + C_{\text{ff}} + C_{\text{r}} + C_{\text{p}} \quad (1)$$

$$232 \quad \Delta_{\text{obs}} C_{\text{obs}} = \Delta_{\text{bg}} C_{\text{bg}} + \Delta_{\text{ff}} C_{\text{ff}} + \Delta_{\text{r}} C_{\text{r}} + \Delta_{\text{p}} C_{\text{p}} \quad (2)$$

233 where subscripts obs, bg, ff, r and p indicate observed, background, fossil fuels,  
 234 respiration, and photosynthesis, respectively, C indicates CO<sub>2</sub> mole fraction in ppm, and  
 235  $\Delta$  indicates  $\Delta^{14}\text{C}$  in ‰. We assume that  $\Delta_{\text{p}}$  is equivalent to  $\Delta_{\text{bg}}$ , since natural  
 236 fractionation during uptake is corrected in the  $\Delta^{14}\text{C}$  measurement and therefore substitute

237  $\Delta_{bg}$  for  $\Delta_p$  in Eq. (2). Then, after solving Eq. (1) for  $C_p$  and substituting this for  $C_p$  in Eq.  
238 (2), we solve Eq. (2) for  $C_{ff}$ , resulting in the following expression for  $C_{ff}$ :

$$239 \quad C_{ff} = \frac{C_{obs}(\Delta_{obs} - \Delta_{bg})}{\Delta_{ff} - \Delta_{bg}} - \frac{C_r(\Delta_r - \Delta_{bg})}{\Delta_{ff} - \Delta_{bg}} \quad (3)$$

240 The value of  $\Delta_{ff}$  is -1000 ‰, since fossil fuels contain no  $^{14}\text{C}$  because they have been  
241 removed from the source of this short-lived radionuclide for millions of years.

242 We use the record from Pt. Barrow, AK (Xiaomei Xu, unpublished data) for the  
243 concurrent background  $\Delta^{14}\text{C}$  values ( $\Delta_{bg}$ ), because [this is the most complete record](#)  
244 [available for the entire time period of this study. The background  \$\Delta^{14}\text{C}\$  record at Pt.](#)  
245 [Barrow, AK is obtained through the UCI/NOAA ESRL \(Earth System Research](#)  
246 [Laboratory\) flask network program that collects whole air samples using 6-L, 1-valve](#)  
247 [stainless steel canisters \(Silco Can, Restek Co.\) that have been pre-evacuated at UCI. The](#)  
248 [canisters are pressurized to ~2 atm using an oil-free pump. Two biweekly samples were](#)  
249 [collected before 2008, and one weekly afterwards. For the period from 17 June 2005 to](#)  
250 [17 March 2006, some duplicate samples were collected using 32-L, 1-valve stainless steel](#)  
251 [canisters. Subsamples were then taken from these samples for  \$^{14}\text{C}\$  analysis.  \$\text{CO}\_2\$  is](#)  
252 [extracted cryogenically at UCI then converted to graphite by the sealed tube zinc](#)  
253 [reduction method \(Xu et al. 2007\). Each sample is ~2.7 mg C in size. Analysis of  \$\Delta^{14}\text{C}\$  is](#)  
254 [performed at the W M Keck AMS facility at UCI with total measurement uncertainty of](#)  
255 [±1.3–2.4‰. Mass dependent fractionation is corrected for using “on-line”  \$\delta^{13}\text{C}\$](#)   
256 [measurements during AMS analysis, which accounts for fractionation that occurred](#)  
257 [during graphitization and inside the AMS. Comparison was made of 22 common sample](#)  
258 [dates spanning 5 yr, of measured  \$\Delta^{14}\text{C}\$  from Barrow between the UCI and the Scripps](#)  
259 [Institution of Oceanography’s  \$\text{CO}\_2\$  Program. It shows differences in measured  \$\Delta^{14}\text{C}\$  are](#)

260 consistent with the reported uncertainties and there is no significant bias between the  
261 programs (Graven et al., 2013). Another inter-comparison is that of AMS-based  
262 atmospheric  $^{14}\text{CO}_2$  measurements organized by the NOAA Earth System Research  
263 Laboratory, Boulder, Colorado. The UCI lab is one the three groups having inter-  
264 laboratory comparability within 1‰ for ambient level  $^{14}\text{CO}_2$  (Miller et al. 2013).  
265 Comparison of the Pt. Barrow data with those from La Jolla (Graven et al., 2012; Fig. 5)  
266 shows good agreement for 2004-2007, when the two data sets overlap. Comparing the  
267 calculated values for  $C_{\text{ff}}$  from these two backgrounds and propagating through the time  
268 series calculations (Section 3.4) results in a difference of approximately 1 % of the signal  
269 we are measuring. We calculate  $C_{\text{bio}}$  (the sum of  $C_r$  and  $C_p$ ) from Eq. (1), using the  
270 calculated values of  $C_{\text{ff}}$  and the independent estimates of  $C_{\text{bg}}$  from the La Jolla data, so  
271 that we understand the contribution of the biosphere to total local emissions.

272 The nuclear power plant contribution, the only other source of  $^{14}\text{C}$ , is small on the  
273 west coast of the U.S. (Graven and Gruber, 2011) and therefore is ignored.

274 Following Turnbull et al. (2006) and Miller et al. (2012), the respiration terms in  
275 the equations above are assumed to reflect contributions due to heterotrophic respiration.  
276 Thus, the second term in Eq. (3) is small in magnitude and is due to heterotrophic  
277 respiration, through which microbes respire  $\text{CO}_2$  that was from carbon previously  
278 incorporated through photosynthesis. This term takes into account the isotopic  
279 disequilibrium due to the significant time delay between photosynthetic incorporation and  
280 respiration, assumed to be 10 years on average (Miller et al., 2012). The magnitude of  
281 this correction for our urban Pasadena site is different relative to sites with smaller  
282 anthropogenic  $\text{CO}_2$  signals, since the  $\text{CO}_2$  photosynthesized into the plant a decade ago

283 was not close to the background air composition of that time but was the local, “polluted”  
284 air. The  $\Delta_r$  in Eq. (3) for each sample was calculated by extrapolating the Pasadena trend  
285 back 10 years. Because of the mild climate in southern California, we used a constant  
286 value of  $C_r = 5$  ppm, the same value used for summer by Turnbull et al. (2006). This  
287 should be taken as an upper limit for this urban region. The range of the correction for  
288 the second term in Eq. (3), including the sign, was  $-0.06 - -0.11$  ppm, generally smaller  
289 relative to regions where the biosphere contribution  $C_r$  is large (Miller et al., 2012;  
290 Turnbull et al., 2006). For the data from the Palos Verdes site, we calculated the  
291 heterotrophic correction term using values of  $\Delta_r$  calculated by extrapolating the Pt.  
292 Barrow background trend back 10 years and used a constant value of  $C_r = 5$  ppm, because  
293 of the mild climate. The correction term for the Palos Verdes data ranged from  $0.20 -$   
294  $0.24$  ppm. The small correction for heterotrophic respiration does not affect any of our  
295 conclusions.

296 In California, there is an added complication when attributing  $\text{CO}_2$  emissions to  
297 fossil fuels using  $\Delta^{14}\text{C}$ . Since 2004, 10 % ethanol has been added to gasoline. The  
298 ethanol contains modern, not fossil, carbon. For gasoline with 10 % ethanol, 6.7 % of the  
299  $\text{CO}_2$  emitted during combustion is from the modern ethanol (EIA, 2015). A correction  
300 for this is made, as discussed in section 2.3.3 below.

301

### 302 **2.3.3 $\delta^{13}\text{C}$ of $\text{CO}_2$**

303 Plots involving the mole fractions and  $\delta^{13}\text{C}$  can be used to determine  $\delta^{13}\text{C}$  of the  
304 local contribution to the observed  $\text{CO}_2$  (Fig. 3). Here we use the Miller-Tans approach  
305 (Miller-Tans approach; MT; Miller and Tans, 2003) for this purpose, since it allows for

306 variations in background composition and we observe a widening difference between the  
307 data for  $\delta^{13}\text{C}$  in Pasadena and the La Jolla background record in recent years (Fig. 3e).

308 The following mass balance equations are used in this analysis:

309  $C_{\text{obs}} = C_{\text{bg}} + C_{\text{src}}$  (4)

310  $\delta_{\text{obs}} * C_{\text{obs}} = \delta_{\text{bg}} * C_{\text{bg}} + \delta_{\text{src}} * C_{\text{src}}$  (5)

311 to give

312  $\delta_{\text{obs}} * C_{\text{obs}} - \delta_{\text{bg}} * C_{\text{bg}} = \delta_{\text{src}}(C_{\text{obs}} - C_{\text{bg}})$  (6)

313 (Miller and Tans, 2003), where the subscript src represents the local source of  $\text{CO}_2$   
314 emissions,  $\delta$  represents  $\delta^{13}\text{C}$ , and the appropriate background values are included for  
315 each sample. Using this formulation (Eq. 6), the slope of the correlation (MT slope)  
316 gives the  $\delta^{13}\text{C}$  of this local source. For this analysis, we calculated the MT slopes for  
317 each month and then determined the seasonal averages, averaging December-January-  
318 February as winter, March-April-May as spring, June-July-August as summer, and  
319 September-October-November as autumn. Seven individual samples, over the eight-year  
320 sampling period in Pasadena, were excluded since they fell more than three times the  
321 standard error from their linear regression best-fit lines. The monthly MT plots for 2011  
322 are shown in Fig. A1, as examples. The very high correlation coefficients ( $R = 0.952 -$   
323  $0.999$ ) suggest that  $\delta_{\text{src}}$  remains constant on time scales of a month. We assume that this  
324 is also the case for the isotopic compositions of petroleum and natural gas combustion,  
325 that we describe below.

326 We use the results from the  $^{14}\text{CO}_2$  calculations for the fraction of  $C_{\text{xs}}$  from the  
327 biosphere ( $F_{\text{bio}} = 1 - F_{\text{ff}}$ ) together with the MT slopes to attribute the  $\text{CO}_2$  derived from

328 petroleum and natural gas combustion ( $C_{\text{pet}}$  and  $C_{\text{ng}}$ ) by mass balance, first by calculating  
329 the  $\delta^{13}\text{C}$  of the fossil fuel component, using:

$$330 \quad \delta_{\text{ff}} = \frac{\delta_{\text{xs}} - \delta_{\text{bio}} * (1 - F_{\text{ff}})}{F_{\text{ff}}} \quad (7)$$

331 where  $F_{\text{ff}}$  is the fraction of  $C_{\text{xs}}$  due to emissions from fossil fuel combustion, as calculated  
332 from the  $^{14}\text{CO}_2$  data. The values for  $\delta_{\text{xs}}$  are the seasonal  $\delta^{13}\text{C}$  values from the MT  
333 analyses and  $\delta_{\text{bio}}$  is taken to be  $-26.6\text{‰}$ , the average  $\delta^{13}\text{C}$  of the ambient air plus the  
334 discrimination of  $-16.8\text{‰}$  for the biosphere (Bakwin et al., 1998). [This value represents](#)  
335 [data from temperate northern latitudes \(28 – 55 °N\), dominated by C3 plants with some](#)  
336 [C4 grasses present \(Bakwin, et al., 1998\). Indeed, grasses in southern California are](#)  
337 [mostly C3 ryes, fescue, and bluegrass, with some C4 grasses such as St. Augustine](#)  
338 [\(www.cropsreview.com/c3-plants.html, last accessed January 25, 2016\).](#) The proportions  
339 of  $\text{CO}_2$  emitted by petroleum and natural gas combustion are calculated using the  $\delta^{13}\text{C}$   
340 values:

$$341 \quad \delta_{\text{ff}} = F_{\text{pet ff}} * \delta_{\text{pet}} + (1 - F_{\text{pet ff}}) * \delta_{\text{ng}} \quad (8)$$

$$342 \quad F_{\text{pet ff}} = \frac{\delta_{\text{ff}} - \delta_{\text{ng}}}{\delta_{\text{pet}} - \delta_{\text{ng}}} \quad (9)$$

343 with an analogous equation for  $F_{\text{ng ff}}$ . where  $F_{\text{pet ff}}$  and  $F_{\text{ng ff}}$  are the fractions of petroleum  
344 and natural gas combustion contributions in  $C_{\text{ff}}$ , respectively. The values of  $\delta_{\text{ng}}$  and  $\delta_{\text{pet}}$   
345 used were  $-40.2 \pm 0.5\text{‰}$  for natural gas (Newman et al., 2008; [covering measurements in](#)  
346 [1972-1973 and 1999](#)) and  $-25.5 \pm 0.5\text{‰}$  for petroleum combustion (average of  
347 measurements in (Newman et al., 2008; [measurements in 2005](#)), and [-26.0, -25.1,](#)  
348 [and -25.5‰ measured in 2007, 2012, and 2014, respectively](#)). The  $C_{\text{ff}}$ ,  $C_{\text{pet}}$ , and  $C_{\text{bio}}$   
349 components were corrected for the presence of 10 % ethanol in California gasoline by

350 multiplying  $C_{\text{pet}}$  by 0.067 (the fraction of  $\text{CO}_2$  emitted by burning the ethanol portion of  
351 the ethanol-gasoline mixture; EIA, 2015) to give the amount, in ppm, of  $\text{CO}_2$  that was  
352 included in  $C_{\text{bio}}$  but should have been attributed to  $C_{\text{pet}}$ . The same amount was deducted  
353 from  $C_{\text{bio}}$ . The magnitude of this correction is 0.5 – 1.2 ppm, averaging 0.84 ppm, which  
354 represents approximately a quarter of the  $C_{\text{bio}}$ , but the latter is very small, averaging 3 – 4  
355 ppm and the correction does not affect our results with respect to  $C_{\text{pet}}$  and  $C_{\text{ng}}$ .  
356

### 357 2.3.4 Time series analysis

358 We used the algorithm of Jiang et al. (2008) to study details of the average annual  
359 patterns of the total  $\text{CO}_2$  and  $C_{\text{ff}}$  in Pasadena, in order to compare with patterns at sites  
360 with less contribution from regional fossil fuel combustion, such as Palos Verdes and La  
361 Jolla background. This method uses the first three Legendre polynomials and harmonic  
362 terms to decompose the signal (Prinn et al., 2000). The harmonic terms define the  
363 seasonal and semi-annual cycles, which we compared to results of the same analysis for  
364 flask data from La Jolla, CA (Keeling et al., 2005).

365 To determine trends in the  $C_{\text{ff}}$  time series, derived from the radiocarbon data, we  
366 used the empirical mode decomposition (EMD) method (Huang et al., 1998; Kobayashi-  
367 Kirschvink et al., 2012). Using this method, nonlinear and nonstationary time series can  
368 be broken down into intrinsic mode functions (IMFs) with increasing period lengths and,  
369 finally, to a long-term trend with at most only one minimum or maximum with slope of  
370 zero. The algorithm involves using cubic splines to calculate maximum and minimum  
371 envelopes for the data series. The average of these envelopes for each time is subtracted  
372 from the original or the previous iteration. This process is repeated until the average is a



373 horizontal line, giving the first IMF. This IMF is subtracted from the raw time series (or  
374 previous starting point) and then repeated until the resulting IMF has only one maximum  
375 or minimum in the series, the long-term trend. High frequency modes are removed first,  
376 with the earliest representing noise. The later modes are interpreted in terms of known  
377 processes, such as annual cycles (e.g., IMFs 3 and 4). Following Wu and Huang (2009),  
378 we added random noise equivalent to the error in the measurements to create 300 time  
379 series, for which the ensemble EMD (EEMD) analyses were averaged. The EEMD  
380 technique is data adaptive, not assuming any shape for the IMFs.

381

### 382 **3 Results and discussion**

383 The purpose of this project was to determine the sources of  $C_{fl}$  in the Los Angeles  
384 basin and compare them with bottom-up inventories and data products from government  
385 agencies and the scientific community. Below, we compare results of source allocation  
386 from the two sites and then examine the temporal variability at the Pasadena site, with its  
387 8-year record. Then we compare the results with government inventories and with the  
388 high-resolution Hestia-LA emissions product.

389

#### 390 **3.1 Spatial variations – comparison of source attribution at the Pasadena** 391 **and Palos Verdes sites**

392 The  $\Delta^{14}C$  time series for the two sites are shown in Fig. 3c and d, 8 years for  
393 Pasadena and 4 years for Palos Verdes. The two data sets are very different, with Palos  
394 Verdes radiocarbon results being significantly higher than those in Pasadena except  
395 during the winter. However, the summer months in Pasadena are characterized by  $\Delta^{14}C$   
396 values far from background, i.e., depleted in  $^{14}C$  due to dilution by  $CO_2$  produced by

Sally Newman 2/19/2016 5:36 PM

Deleted: CO<sub>2</sub> emissions

398 burning of fossil fuels containing none of the radioactive isotope. There are occasional  
399 negative spikes in  $\Delta^{14}\text{C}$  during the winter. Total  $\text{CO}_2$  excess ( $C_{\text{xs}}$ ; Fig. 4), determined as  
400  $\text{CO}_2$  concentration minus background, is similarly disparate with respect to timing. The  
401 total enhancement at both Pasadena and Palos Verdes,  $C_{\text{xs}}$ , spikes during winter (up to 65  
402 ppm and 34 ppm, respectively), but the Pasadena excess also peaks during the summer  
403 (up to 43 ppm), whereas Palos Verdes values for  $C_{\text{xs}}$  are at a minimum during the warm  
404 months (3-20 ppm). When the  $^{14}\text{C}$  and  $C_{\text{xs}}$  information are combined to calculate  $\text{CO}_2$   
405 emissions due to fossil fuels ( $C_{\text{ff}}$ ; eqn. 3; Fig. 4), we see summer maxima for  $C_{\text{ff}}$  in  
406 Pasadena, but not in Palos Verdes. The spikes in  $C_{\text{xs}}$  and  $C_{\text{ff}}$  during fall and winter  
407 seasons are not the general trend in Pasadena, as evidenced by the quarterly averages  
408 (Fig. 6b). The amount of  $C_{\text{ff}}$  in the Pasadena seasonal averages (Fig. 4a, 6b) ranges from  
409  $(18.9 \pm 1.2)$  ppm (winter) to  $(26.8 \pm 0.4)$  ppm (summer). In Palos Verdes,  $C_{\text{ff}}$  averages  $(5$   
410  $\pm 3)$  ppm during the warmer months and  $(12 \pm 5)$  ppm during the winter months (Fig.  
411 4b). However,  $\text{CO}_2$  emissions from the biosphere ( $C_{\text{bio}}$ ) tend to be higher during the  
412 cooler months at both sites (Fig. 4). [Refer to Section 3.2 for more discussion of the](#)  
413 [biosphere's contribution to  \$C\_{\text{xs}}\$  in Pasadena.](#)

414 The explanation for the differences in the seasonal cycles of  $C_{\text{xs}}$  and  $C_{\text{ff}}$  at the two  
415 sites is probably the different wind patterns for the different times of year. Figure 7  
416 shows back trajectories ending at 1400 PST in Pasadena (Fig. A2 for both sites),  
417 calculated using NOAA's HYSPLIT model (Draxler and Rolph, 2014; Rolph, 2014), for  
418 January and July 2011. These are representative of these months in all years of this  
419 study. Wind directions during July are from the west-southwest, whereas they are mostly  
420 from the northeast but much more varied during the winter. Thus, in Pasadena, elevated

421  $C_{xs}$  and  $C_{ff}$  values during the summer result from air masses traveling across the Los  
422 Angeles basin, picking up emissions and transporting them inland. During the winter, the  
423 airflow is more mixed, resulting in lower average  $C_{ff}$  signals in Pasadena, since a  
424 significant proportion of the winds bring less polluted air from the much less populated  
425 mountains and deserts located to the north (Santa Ana winds) (Fig. 7). The summer  
426 westerly winds bring ocean air to the Palos Verdes site, characterized by  $CO_2$  mole  
427 fractions and  $\Delta^{14}C$  very similar to background marine air. During the cooler months, the  
428 Santa Ana winds from the northeast occasionally blow over the LA basin, bringing its  
429 emissions to the coastal site (Fig. 7). This pattern results in more scatter in the magnitude  
430 of  $CO_2$  excess observed during the winter at the Palos Verdes site, than during the  
431 summer. Figure 8 shows the average annual pattern for  $C_{ff}$  at the two sites,  
432 demonstrating the effect of the varying wind direction patterns.

433

### 434 **3.2 Attribution of $CO_2$ excess from different anthropogenic sources for** 435 **Pasadena**

436 Since we have information regarding the relative contributions of fossil fuel  
437 combustion and biosphere respiration from the radiocarbon data, we can use the  
438 differences in the  $\delta^{13}C$  of the  $CO_2$  to look at the contributions of petroleum/gasoline  
439 versus natural gas combustion. We use the MT approach to distinguish between different  
440 fossil fuel sources of  $CO_2$  (Miller and Tans, 2003). As described in section 2.3.3, the MT  
441 slope of the correlation gives the  $\delta^{13}C$  of the local source of  $CO_2$  emissions. In many  
442 cases it is difficult to distinguish the anthropogenic sources because the biosphere's  
443 signal can overlap that of petroleum. However, in a megacity such as the Los Angeles

444 basin, the contribution of the biosphere to the total CO<sub>2</sub> enhancement can be minimal  
445 ( $\leq 20\%$  in Pasadena; Newman et al., 2008; Newman et al., 2013) during the afternoon,  
446 when the boundary layer is deepest and most thoroughly mixed. In this study, we use the  
447 information from  $\Delta^{14}\text{C}$  presented above to further constrain the biosphere's input. Since  
448 the other major anthropogenic sources (cement production and combustion of coal) are  
449 not present in the Los Angeles basin,  $\delta^{13}\text{C}$  from MT plots can be used to differentiate the  
450 proportions of natural gas and oil burned in the region, as discussed below.

451 Seasonal MT slopes for the mid-afternoon Pasadena samples from 2006 through  
452 2013 are shown in Fig. 6a. We do not present similar analysis for the Palos Verdes data  
453 because it is a shorter data set, with only 3-5 measurements per month (12 per season),  
454 and the range in CO<sub>2</sub> mole fractions during the warmer months is less than 20 ppm for all  
455 spring and summer seasons. Thus there are insufficient meaningful data to produce a  
456 significant trend. Vardag et al. (2015) came to this same conclusion for a rural site in  
457 Germany, based on a modeling study.

458 The  $\delta^{13}\text{C}$  values from MT regressions for the cooler portions of the year in  
459 Pasadena are almost always higher than those for the warmer portions. The values for the  
460 cooler seasons average  $(-30.6 \pm 0.5)\text{‰}$ ,  $1.8\text{‰}$  higher than the average for the warmer  
461 months,  $(-32.4 \pm 0.6)\text{‰}$ . Assuming that there is no contribution from respiration and  
462 that the  $\delta^{13}\text{C}$  of the high-CO<sub>2</sub> end members are  $-40.2\text{‰}$  for natural gas and  $-25.5\text{‰}$  for  
463 petroleum combustion, as discussed above, then the proportion of natural gas burned in  
464  $C_{\text{xs}}$  is 32 % during the cooler months and 45 % during the warmer months. The larger  
465 fraction of natural gas burned during the warm part of the year is consistent with the  
466 observed burning of more natural gas for electricity generation during summer months, as

Sally Newman 2/19/2016 10:02 AM

**Deleted:** Newman et al. (2008) showed that no biospheric input was required to explain the  $\delta^{13}\text{C}$  of mid-afternoon CO<sub>2</sub> during 1972-73 and 2002-2003, although up to 20 % was allowed by the uncertainties.

472 would be required to power air conditioning needs. Mild winters in this climate require  
473 less natural gas combustion for heating buildings, thus minimizing a large winter peak  
474 frequently seen in colder regions, such as Salt Lake City, UT (Pataki et al., 2003; Bush et  
475 al., 2007) and Chicago, IL (Moore and Jacobson, 2015). This attribution of the different  
476 contributions to  $C_{ff}$  still does require knowledge of the  $\delta^{13}C$  value of the biosphere. As  
477 mentioned above, we use a discrimination of 16.8 ‰, the average determined by Bakwin  
478 et al. (1998) for northern mid-latitudes and includes a mix of C3 and C4 metabolism  
479 plants, dominated by C3. More C4 plants will raise the  $C_{ng}$  curve and lower the  $C_{pet}$   
480 curve, since the discrimination by C4 plants is much lower (Farquhar et al., 1989).

481 As mentioned above, we can use the information provided by the  $^{14}CO_2$  data to  
482 put better constraints on contributions from the biosphere. The calculations based on  
483  $\Delta^{14}C$  data in Fig. 6b show that the maximum biosphere contribution was during winter  
484 2012-2013, 7 ppm (28 % of the total  $C_{ff}$ ), and the minimum was 0.1 ppm during spring of  
485 2010. The average is  $(4.1 \pm 0.5)$  ppm (16 % of  $C_{ff}$ ) during cooler months and  $(2.2 \pm 0.3)$   
486 ppm (8 % of  $C_{ff}$ ) during warmer months. The seasonality could be due to variations in  
487 emissions from the biosphere. However, it is probably due to a more complex  
488 combination of emissions and uptake.

489 The observation that there are seasonal patterns to the  $CO_2$  emissions from  
490 combustion of petroleum and natural gas has implications for the effective composition  
491 of  $\Delta^{14}C$  from fuel combustion. The value for fossil fuels is taken to be -1000 ‰, since  
492 they contain no  $^{14}C$ . However, because we have 10 % modern ethanol in our gasoline,  
493 and there is seasonal variation in the ratio of gasoline to natural gas usage, there is  
494 actually a seasonal variation in radiocarbon from the bulk fuel combustion component.

Sally Newman 2/19/2016 10:05 AM

**Deleted:** emissions

Sally Newman 2/19/2016 10:05 AM

**Deleted:** emissions

Sally Newman 2/19/2016 10:05 AM

**Deleted:** emissions

498 And at no time is the  $\Delta^{14}\text{C}$  value actually that of pure fossil fuel (-1000 ‰). The average  
499 value is -954 ‰, and spring-summer periods average 33 ‰ higher than autumn-winter  
500 (-939 – -972 ‰, respectively). These seasonal and overall values for  $\Delta^{14}\text{C}$  of the fuel  
501 component were determined as the best-fit values from the individual  $C_{\text{ff}}$  data to the  
502 seasonal mass balance calculations of  $C_{\text{pet}}$  and  $C_{\text{ng}}$ .

503

### 504 **3.3 Average seasonal and semi-annual patterns**

505 The emissions of  $\text{CO}_2$  by anthropogenic processes significantly modifies the  
506 annual cycle of  $\text{CO}_2$  observed in the Los Angeles region relative to the oceanic air that  
507 enters the basin, as exemplified by the background air sampled in La Jolla, CA (Keeling  
508 et al., 2005; see discussion in section 2.3.1). There is very little seasonal variability in  
509 Pasadena (Fig. 9a). Whereas the average background annual cycle is characterized by a  
510 peak in April and drawdown in August-September, with an amplitude of 11 ppm (Fig.  
511 9g), the Pasadena cycle is noisy and relatively flat, with lower  $\text{CO}_2$  mole fractions in  
512 January-April and high values the rest of the year and only an amplitude of 5 ppm (Fig.  
513 9a). Each pattern can be modeled well using the Legendre polynomial/harmonic analysis  
514 of Jiang et al. (2008; Fig. 9b, h). The sum of the seasonal and semi-annual harmonic  
515 terms reproduces the data very well, with  $r^2$  values of 0.70 and 0.91 for Pasadena and  
516 background, respectively. The average annual cycles are 6 months out of phase, whereas  
517 the semi-annual oscillation cycles look very similar at the two sites. The seasonal cycle  
518 in Pasadena is consistent with influx of combustion  $\text{CO}_2$  during the hot summer months  
519 due to increased burning of natural gas at power plants located dominantly in the  
520 southwestern portion of the LA basin (CEC, 2015). In contrast, the background data

Sally Newman 2/19/2016 10:08 AM  
Deleted: R<sup>2</sup>

522 reflect global patterns with a drawdown in CO<sub>2</sub> during the summer growing season in the  
523 northern hemisphere. Jiang et al. (2012) concluded that the semi-annual oscillation at  
524 NOAA's GLOBAL-VIEW sites is due to the combination of gross primary production  
525 and respiration of the biosphere. During the winter season, photosynthesis is largely  
526 reduced. The peak for gross primary production is relatively flat in winter. However,  
527 CO<sub>2</sub> is still emitted to the atmosphere by respiration from the biosphere in winter, which  
528 has a relatively sharp peak compared with the photosynthesis term. Thus the  
529 combination of gross primary production and respiration leads to the double peaks in  
530 each year in the net ecosystem production, which contributes to the semi-annual  
531 oscillation in CO<sub>2</sub> (Jiang et al., 2012). The semi-annual oscillation in the background  
532 signal is consistent with this interpretation. We see virtually the same pattern in  
533 Pasadena, although the amplitude is smaller, consistent with the small biospheric  
534 contribution indicated by the  $\Delta^{14}\text{C}$  results.

535         Based on the work of Jiang et al. (2012) we expect the annual cycle in Pasadena  
536 to be larger in amplitude than in La Jolla since it is further north, but the amplitude is  
537 actually much smaller. If the regional emissions of CO<sub>2</sub> in Pasadena are relative to a La  
538 Jolla background, then there is a huge enhancement during the summer! Indeed, the  
539 seasonal cycle for C<sub>fr</sub> (Fig. 8) is 11 ppm, with the peak in August-September, and there is  
540 very little semi-annual oscillation.

541         The annual pattern for CO<sub>2</sub> in Palos Verdes is also heavily influenced by the  
542 transport of combustion emissions from the Los Angeles basin (Fig. 7, 8, 9c, d). The  
543 average monthly pattern is more similar to the background's (Fig. 9g, h) than to  
544 Pasadena's (Fig. 9a, b). However, there is a strong peak in the winter that is consistent

545 with the increased number of days during this time of year with winds from the north to  
546 east, travelling over the basin. Doing the same analysis for the monthly minimum values  
547 (Fig. 9e, f) gives a pattern that is much more similar to the background's, confirmed by  
548 the comparison of the raw data with the background smoothed time series in Fig. 3. This  
549 supports use of minimum values from Palos Verdes as reasonable background for the Los  
550 Angeles basin. The  $C_{ff}$  annual pattern is inverse to that in Pasadena, as expected by the  
551 seasonal wind patterns (Figs. 7, 8).

552 The conclusion of this analysis of the annual cycles is that the Pasadena  $CO_2$   
553 pattern is significantly different from the natural cycles observed in La Jolla background  
554 and show very little seasonal variation compared with this background. The semi-annual  
555 pattern, although smaller in amplitude than expected, is in phase with that observed in the  
556 background, which we suggest might reflect a reduced biosphere signature in Pasadena  
557 due to artificial irrigation, which may reduce seasonality expected due to wet and dry  
558 parts of the year. Both the Pasadena and Palos Verdes average  $CO_2$  patterns reflect the  
559 seasonal changes in wind patterns, whereas the monthly minimum Palos Verdes pattern is  
560 that expected for the background air entering the LA basin. It will be interesting to see  
561 whether water restrictions put into effect during summer of 2015 because of an on-going,  
562 severe drought (ca.gov/drought, 2015), affect the patterns observed in the future.

563

564

### 565 **3.4 Temporal trends in $CO_2$ excess observed in Pasadena**

#### 566 **3.4.1 Long-term time series analysis**

567 In order to discern the long-term trends in fossil-fuel  $CO_2$  excess, we must first  
568 remove noise and the periodic signals discussed above from the record. We used



569 empirical mode decomposition (EEMD; Huang et al., 1998; Kobayashi-Kirschvink et al.,  
570 2012), as described in the calculation section above, on the 8-year time series of  $C_{ff}$  (Fig.  
571 4a) to identify intrinsic mode functions (IMFs; summary in Fig. 10a-d; full results in Fig.  
572 A3). The noise is represented by the first and second modes (IMF 1 and IMF 2).  
573 Combination of the third and fourth modes of the  $C_{ff}$  time series (IMF 3 and IMF 4)  
574 correlates significantly with the 30-day average record for temperature measured at the  
575 top of the 9-story library next to the sampling site ( $r^2 = 0.6$ ). Note that there are severe  
576 mode mixing problems in IMF3 (e.g. during 2011–2013) between the dominant annual  
577 cycle and subseasonal variations, which also affects the nonlinear decompositions in the  
578 higher modes. To minimize the effects of mode mixing on the extractions of inter-annual  
579 trends, we perform the EEMD again after removing the average annual cycle (minus the  
580 mean of the raw data), defined as monthly averages over the entire time period (2006-  
581 2013; resulting time series shown in Fig. 10e). The revised inter-annual trend is shown in  
582 Fig. 10f. The sum of the trend + IMF 6 is a curve with increasing  $C_{ff}$  values leading up to  
583 mid-2007, when they began to fall, until leveling off in 2010 and perhaps starting to rise  
584 towards the end of the time series. There are end effects in this method, such that we do  
585 not have confidence in the first and last years of the analysis. The uncertainties in this  
586 calculation are shown by the shaded regions in Fig. 10f. These were determined as the  
587  $1\sigma$  standard deviations of adding random noise equivalent to 13.7 % to the data 300 times  
588 and then running the EMD analysis. The 13.7 % noise added is the uncertainty of the  $C_{ff}$   
589 values calculated from  $\Delta^{14}C$ ,  $\pm 1$  ppm, relative to the standard deviation of the data, 7.3  
590 ppm. The maximum and minimum values are distinct at approximately the  $2\sigma$  standard  
591 deviation level, as shown in Fig. 10f and indicate a significant decrease of 9.5 % between

Sally Newman 2/19/2016 10:08 AM

Deleted: R<sup>2</sup>

593 | the maximum in May 2007, and the average for January-June 2010. Using different  
594 | backgrounds for  $\Delta^{14}\text{C}$ , such as extrapolating the data from La Jolla (Fig. 5) does not  
595 | significantly affect this analysis, resulting in differences of  $(0.01 \pm 0.09)$  ppm  $C_{\text{ff}}$  out of a  
596 | range on the order of 2 ppm. And our result showing that there are different values of  
597 |  $\Delta^{14}\text{C}$  for bulk fuel for autumn-winter than for spring-summer also does not change these  
598 | conclusions, since the RMSE of the IMF6+trend (Fig. 10f) using different  $\Delta^{14}\text{C}$  for cool  
599 | vs. summer months relative to the constant average value is 0.1 ppm  $C_{\text{ff}}$ .

600 | The timing of the drop in the fossil-fuel  $\text{CO}_2$  excess around 2008 is consistent  
601 | with the economic recession in late 2007-2009 (NBER, 2010) with slow recovery  
602 | beginning in 2010. Similar results for global  $\text{CO}_2$  emissions due to fossil fuel combustion  
603 | have been documented by Peters et al. (2012) and Asefi-Najafabady et al. (2014). The  
604 | fraction of decrease in  $C_{\text{ff}}$  (9.5 %) is similar to, although less than, the decrease in global  
605 | GDP during this time (global GDP decreased by 13 %; World Bank, 2015).

### 607 | **3.4.2 Comparison with inventories and bottom-up gridded $C_{\text{ff}}$ data**

608 | A major goal of this study is to compare trends in top-down measurements such  
609 | as those described here with bottom-up estimates in order to understand how to bring  
610 | them together in space and time for direct validation. Annual averages of the seasonal  
611 | amounts derived for  $C_{\text{ff}}$ ,  $C_{\text{pet}}$ , and  $C_{\text{ng}}$  compare well in relative proportions to the averages  
612 | from California's state inventory provided by the California Air Resources Board  
613 | (CARB, 2015). Annual values for  $\text{CO}_2$  emissions from all fossil fuels, on-road  
614 | transportation, and natural gas consumption for the entire state of California, through  
615 | 2013, are superimposed on the seasonal averages for  $C_{\text{ff}}$ ,  $C_{\text{pet}}$ , and  $C_{\text{ng}}$  in Fig. 11. The

Sally Newman 2/21/2016 11:18 PM

**Deleted:** (average from Fig. 10a plus the maximum in Fig. 10f: 23.7 ppm)

Sally Newman 2/21/2016 11:18 PM

**Deleted:** (average from Fig. 10a plus the average of minimum six-month period from Fig. 10f: 21.4 ppm)

Sally Newman 2/19/2016 5:15 PM

**Deleted:** The observation that  $C_{\text{ff}}$  does not decrease by as large a percentage as the economy is consistent with the analysis of York (2012) that anthropogenic emissions are asymmetric with respect to economic growth and decline. Increases in emissions that come during growth periods are not matched by declines of the same magnitude during economic downturns, because high consumption durable goods that are put in operation during growth remain in use during the decline.

Sally Newman 2/19/2016 5:40 PM

**Deleted: emissions d**

634 decrease in total fossil fuels combustion between 2007 and 2011 in the State's inventory  
635 is 11 %, very similar to the 9.5 % decrease indicated by the EEMD time series analysis of  
636 our  $C_{ff}$  results above. There is a difference in timing between the data presented here  
637 (2010) and those from the CARB inventory (2011-2012) that may be due to uncertainties  
638 in the data or to the different domains covered by the two data sets. The relative  
639 proportions of the on-road portion of the CARB budget is 57 % of fossil fuel  $CO_2$   
640 emissions and the petroleum portion of our top-down estimate averages 54 % of  $C_{ff}$ . This  
641 inventory is for the entire state, not the LA basin, and it includes annual values only.  
642 This discussion has focused on inter-annual variations in  $C_{ff}$ , although, as we have shown  
643 in Fig. 7 and 8, there are at least seasonal variations in wind direction. Looking at back  
644 trajectories from the entire time period of this study, we see no significant shifts in the  
645 winds, from year to year although systematic modeling has not yet been done and is  
646 beyond the scope of this paper. Next, we look at finer spatial and temporal scales.

647 Seasonal variations in  $C_{pet}$  concentration at the Pasadena location can be  
648 compared to the variation in emissions compiled by various sources. Figure 12 presents a  
649 comparison of the  $C_{pet}$  concentration to the petroleum and on-road  $CO_2$  emissions  
650 components estimated by the Energy Information Administration (EIA) (EIA, 2015), the  
651 State of California (CARB, 2015), and the Hestia-LA project (K. R. Gurney, personal  
652 communication). Comparison of the seasonal averages for petroleum consumption data,  
653 based on deliveries (EIA), and gasoline taxes collected (CBE, 2014) with  $C_{pet}$  indicates  
654 similar decreases of 10-20 %, but with a lag of a few months (Fig. 12). The lag could be  
655 due to the different domains of the data sets: EIA and State of California data reflect the

Sally Newman 2/19/2016 5:41 PM

Deleted: emissions

657 | entire state domain while the Hestia  $C_{ff}$  data product reflects the LA Basin specifically,  
658 | and the atmospheric data presented here represents air sampled in Pasadena.

659 | To truly understand the observations in Pasadena, we must combine information  
660 | from spatial and temporal meteorological and  $C_{ff}$  databases, such as obtained using a  
661 | model like the Weather Research and Forecasting (WRF) model. Since this is beyond the  
662 | scope of this work, we have used the information from HYSPLIT back trajectories (Fig.  
663 | 7; January and July) to provide rough limits for winds arriving in Pasadena at our  
664 | sampling time of 14:00 PST. These back trajectories suggest that prevailing winds  
665 | during the summer come from the southwest, across the basin, and winds during the  
666 | winter come from the northeast, across the mountains from the desert. We have looked at  
667 | 1.3-km x 1.3-km gridded  $C_{ff}$  from the Hestia-LA data product to qualitatively determine  
668 | what relative emissions from petroleum combustion are expected during January and July  
669 | for the two years of the Hestia data (2011 and 2012). These are plotted in Fig. 12 and  
670 | agree in seasonality with the observations presented here; more  $C_{pet}$  is observed during  
671 | the summer than during the winter. A map of the regions selected for January (NE) and  
672 | July (SW) is presented in Fig. 13a, along with the HYSPLIT back trajectories for January  
673 | and July, 2011, and the monthly average  $CO_2$  emissions due to total petroleum  
674 | combustion (the Hestia-LA product) from the two integrated areas based on the wind  
675 | directions are shown in Fig. 13b for years 2011 and 2012.

676 | We show comparison of the  $C_{ng}$  results from Pasadena with area-integrated  
677 | bottom-up inventories and the Hestia-LA data product in Fig. 14. The California Energy  
678 | Commission (CEC, 2015) compiles data for natural gas consumed by power plants  
679 | throughout the state, including Los Angeles and Orange counties. These seasonal data

Sally Newman 2/19/2016 5:42 PM  
**Deleted:** emissions

Sally Newman 2/21/2016 11:42 PM  
**Deleted:** Furthermore, the EIA data and the gasoline tax-based data will likely be displaced in space and time from the point of combustion, which is dominated by on-road vehicles. The Hestia data, by contrast, is a fossil fuel  $CO_2$  emissions data product specific in space and time to the individual building and road segments (Gurney et al., 2012).

Sally Newman 2/19/2016 5:43 PM  
**Deleted:** emissions

Sally Newman 2/19/2016 5:43 PM  
**Deleted:** emissions

691 are consistent with the detailed Hestia-LA data for the electricity production for the entire  
692 Los Angeles basin (dashed dark blue line in Fig. 14a). And the seasonality of all of the  
693 inventories involving just the electrical power sector agrees well with the seasonality of  
694 the time series for  $C_{ng}$  (Fig. 14a), with peaks during the summer and troughs during the  
695 winter. The source attribution analysis using  $\Delta^{14}C$  and  $\delta^{13}C$  also captures the increase in  
696  $C_{ng}$  consumption of the power plants in recent years, although the data from this study  
697 suggest that the increase started earlier than do the inventories. However, the  
698 observations of  $CO_2$  concentration and  $\delta^{13}C$  integrate over all natural gas combustion and  
699 cannot pick out just this one sector.

700 Overall statewide and Los Angeles basin inventories show maximum natural gas  
701 usage during the winter (dashed green line in Fig. 14b). Other sources of combusted  
702 natural gas include residential, commercial, industrial, and transportation use, which  
703 could affect the trends, but we do not have seasonal data for these in the Los Angeles  
704 megacity for the full period of this study. However, the seasonal signal for total  
705 emissions from natural gas combustion from the Hestia-LA project for 2011-2012 is  
706 consistent with the data presented here, when the seasonal prevailing wind directions are  
707 considered. The seasonal pattern of emissions from natural gas combustion at any one  
708 location is characterized by a small peak during the cooler months and a trough during  
709 the warmer months (Fig. 13c). However,  $C_{ff}$  in the region sampled by winds arriving in  
710 Pasadena during the winter (the northeast) are always lower than those in the basin, over  
711 which the summer winds travel to the sampling site. Therefore, transport of air masses  
712 following the seasonal wind patterns can explain the observations in Pasadena. The  
713 earlier onset of the increase in  $C_{ff}$  from natural gas combustion indicated by the data

Sally Newman 2/19/2016 5:43 PM  
**Deleted:** emissions

715 | (2010) relative to that indicated by the government inventories might be due to the  
716 | mismatch in geographical regions, variations in inter-annual atmospheric transport, or  
717 | deficiencies in the inventories.

718 |         Since the seasonal cycle observed in  $C_{\text{pet}}$  and  $C_{\text{ng}}$  in Pasadena is probably due to  
719 | atmospheric transport, modeling of this effect is critical to being able to combine top-  
720 | down observations and bottom-up economic and usage data for a direct consistency  
721 | comparison. These effects must be removed in order to understand long-term trends due  
722 | to variations in anthropogenic emissions. The time series analysis using Empirical Mode  
723 | Decomposition presented in section 3.4.1 removes the seasonal signals to concentrate on  
724 | the longer-term signals, which show reasonable agreement with the longer-term trends in  
725 | the statewide inventory.

726

#### 727 | **4 Conclusion**

728 |         Detection of anthropogenic excess of  $\text{CO}_2$  at two sites in the Los Angeles basin,  
729 | one on the coast and one inland against a barrier mountain range, reveals significant  
730 | spatial and seasonal variability due to the biosphere, natural gas combustion, and  
731 | petroleum combustion. Seasonal patterns in wind direction determine the source region  
732 | of the excess detected at the two sites. Winds from the west to southwest during the  
733 | warmer months bring marine air with little excess to Palos Verdes, and these same winds  
734 | continue across the LA basin picking up emissions from fossil fuel combustion to be  
735 | observed in Pasadena. During the cooler months, wind directions are more varied and  
736 | include periods when air with low emissions comes to Pasadena from the northeast to

737 northwest and then travels across the basin to Palos Verdes, incorporating anthropogenic  
738 emissions along the way.

739         The nature of the excess changes with season, as reflected by the  $\delta^{13}\text{C}$  values of  
740  $\text{CO}_2$  observed in Pasadena. During warmer months, lower values for  $\delta^{13}\text{C}$  of the local  
741 excess indicate a higher proportion of natural gas burned, consistent with government  
742 inventories that indicate more natural gas burned during summer to produce electricity to  
743 power air conditioning. Even more importantly, however, the seasonal trends in the  
744 fossil fuel combustion observed in Pasadena are consistent with the shift from  
745 southwesterly winds during warmer months to northeasterly winds during cooler months.  
746 Therefore the source region of emissions changes from the Los Angeles basin during  
747 summer to the mountains and desert during winter, for our Pasadena sampling site.  
748 Trend analysis by ensemble empirical mode decomposition supports the relationship  
749 between emissions and temperature.

750         The long-term trend in  $\text{CO}_2$  excess from fossil fuel combustion is consistent with  
751  $C_{\text{fit}}$  changes associated with the economic recession and slow recovery of 2008 through  
752 the present, and indicates a significant decrease of 9.5 % since the maximum in late 2007,  
753 consistent with the bottom-up inventory of the California Air Resources Board. Indeed,  
754 top-down and bottom-up methods of determining the anthropogenic sources of  $\text{CO}_2$   
755 emissions must be compared to each other to better understand inconsistencies, potential  
756 biases, and uncertainty. Previously, however, comparisons have been limited by the  
757 scope of emissions, large and overlapping uncertainty, and differences in the target  
758 domain. Here we have shown that combining data from radiocarbon and  $\delta^{13}\text{C}$  values  
759 moves us towards a direct comparison in a megacity with very large emissions.

Sally Newman 2/19/2016 5:44 PM  
**Deleted:** emissions

761 Measurement trends at a receptor site are consistent with annual variations in California  
762 statewide bottom-up inventories for  $C_{gr}$  attributed to petroleum and natural combustion,  
763 individually as well as for total CO<sub>2</sub> emissions. Even greater consistency between top-  
764 down measurements and granular emission estimates specific for the LA megacity  
765 domain are achieved when considering wind direction and sub-city source regions. This  
766 strengthens the need to have measurement, modeling, and inventories that are specifically  
767 aimed at the same domain with fine space/time resolution.

768 The next steps are to include modeling with inversion of the measurements to  
769 understand the combination of atmospheric transport and emissions and to extend the  
770 analysis to a denser network of surface monitoring stations such as the Los Angeles  
771 Megacities Carbon Monitoring Project (Kort et al., 2013) and the California Laboratory  
772 for Atmospheric Remote Sensing (CLARS) observations from Mount Wilson (Wong et  
773 al., 2015). Although the uncertainties are large enough that the method described here  
774 will not be usable in non-urban regions, similar to the conclusion of the modeling study  
775 by Vardag et al. (2015), anthropogenic  $C_{gr}$  dominate significantly over natural processes  
776 in megacities. Therefore, this kind of monitoring in megacities will allow society to  
777 understand and monitor the sources of the CO<sub>2</sub> that are the major contributors to global  
778 warming.

## 779 **Acknowledgments**

780 This work would not have been possible without support from the W.M. Keck Carbon  
781 Cycle Facility at UCI. We specifically thank J. Southon for his help with sample  
782 analysis. We acknowledge funding from the Keck Institute for Space Studies, NASA  
783 Grant NNX13AC04G, and NASA Grant NNX13AK34G. We also acknowledge funding

Sally Newman 2/19/2016 5:45 PM

**Deleted:** CO<sub>2</sub> emissions

Sally Newman 2/19/2016 5:45 PM

**Deleted:** emissions



786 from the California Air Resources Board Contract #13-329. The statements and  
787 conclusions in this report are those of the Contract and not necessarily those of the  
788 California Air Resources Board. The mention of commercial products, their source, or  
789 their use in connection with materials reported herein is not to be construed as actual or  
790 implied endorsement of such products. The authors gratefully acknowledge the NOAA  
791 Air Resources Laboratory (ARL) for providing the HYSPLIT transport and dispersion  
792 model used in this publication. We thank N. C. Shu for hosting the site on the Palos  
793 Verdes peninsula.

794 **References**

- 795 [Andres, R. J., Boden, T. A., Bréon, F. M., Ciais, P., Davis, S., Erickson, D., Gregg, J. S.,](#)  
796 [Jacobson, A., Marland, G., Miller, J., Oda, T., Olivier, J. G. J., Raupach, M. R., Rayner,](#)  
797 [P., and Treanton, K.: A synthesis of carbon dioxide emissions from fossil-fuel](#)  
798 [combustion, Biogeosciences, 9\(5\), 1845–1871, doi:10.5194/bg-9-1845-2012, 2012.](#)
- 799 Affek, H. and Eiler, J.: Abundance of mass 47 CO<sub>2</sub> in urban air, car exhaust, and human  
800 breath, *Geochim Cosmochim Acta*, 70(1), 1–12, 2006.
- 801 Asefi-Najafabady, S., Rayner, [P. J.](#), Gurney, [K. R.](#), McRobert, [A.](#), Song, [Y.](#), Coltin, [K.](#),  
802 [Huang, J.](#), Elvidge, [C.](#), and Baugh, [K.](#): A multiyear, global gridded fossil fuel CO<sub>2</sub>  
803 emission data product: Evaluation and analysis of results, *J Geophys. Res-Atmos*, 119,  
804 10,213-10,231, doi:10.1002/2013JD021296, [2014](#).
- 805 Bakwin, P., Tans, P., White, J. and Andres, R.: Determination of the isotopic (<sup>13</sup>C/<sup>12</sup>C)  
806 discrimination by terrestrial biology from a global network of observations, *Global*  
807 *Biogeochem Cycles*, 12, 555-562, 1998.
- 808 Bush, S., Pataki, D., and Ehleringer, J.: Sources of variation in δ<sup>13</sup>C of fossil fuel  
809 emissions in Salt Lake City, USA, *Appl. Geochem*, 2, 715-723, doi:  
810 10.1016/j.apgeochem.2006.11.001, [2007](#).
- 811 CARB, California Air Resources Board: available at:  
812 <http://www.arb.ca.gov/cc/inventory/data/data.htm> (last access: July 2015), 2015.
- 813 CBE, California Board of Equalization: available at:  
814 [http://www.boe.ca.gov/sptaxprog/reports/MVF\\_10\\_Year\\_Report.pdf](http://www.boe.ca.gov/sptaxprog/reports/MVF_10_Year_Report.pdf) (last access:  
815 November 2014), 2014.
- 816 CEC, California Energy Commission: available at:  
817 [http://energyalmanac.ca.gov/electricity/web\\_qfer/Power\\_Plant\\_Statistical\\_Information.p](http://energyalmanac.ca.gov/electricity/web_qfer/Power_Plant_Statistical_Information.p)  
818 [hp](#) (last access: January 2015), 2015.
- 819 Clark-Thorne, S. and Yapp, C.: Stable carbon isotope constraints on mixing and mass  
820 balance of CO<sub>2</sub> in an urban atmosphere: Dallas metropolitan area, Texas, USA, *Applied*  
821 *Geochemistry*, 18(1), 75–95, 2003.
- 822 [Coplen, T. B.: Editorial: more uncertainty than necessary, \*Paleoceanography\*, 11, 369-](#)  
823 [370, 1996.](#)
- 824 Djuricin, S., Pataki, D. E. and Xu, X.: A comparison of tracer methods for quantifying  
825 CO<sub>2</sub> sources in an urban region, *J Geophys Res-Atmos*, 115, D11303,  
826 doi:10.1029/2009JD012236, 2010.
- 827 Draxler, R.R. and Rolph: G.D.: HYSPLIT (HYbrid Single-Particle Lagrangian Integrated  
828 Trajectory) Model access via NOAA ARL READY Website  
829 (<http://www.arl.noaa.gov/HYSPLIT.php>). NOAA Air Resources Laboratory, College

- 830 Park, MD, 2014.  
831  
832 Duren, R. M. and Miller, C. E.: Measuring the carbon emissions of megacities, *Nature*  
833 *Climate Change*, 2(8), 560–562, 2012.
- 834 EDGAR: European Commission, Joint Research Centre (JRC)/Netherlands  
835 Environmental Assessment Agency (PBL). Emission Database for Global Atmospheric  
836 Research (EDGAR), release version 4.0. <http://edgar.jrc.ec.europa.eu> (last access:  
837 September 2015), 2009.
- 838 EIA (U.S. Energy Information Agency): Frequently asked questions: available at:  
839 <http://www.eia.gov/tools/faqs/faq.cfm?id=307&t=11>, last access 4 September 2015.
- 840 [Farquhar, G., Ehleringer, J. R., and Hubick, K. T.: Carbon isotope discrimination and](#)  
841 [photosynthesis, \*Annu. Rev. Plant. Phys. Plant Mol. Biol.\*, 40, 503–537, 1989.](#)
- 842 Graven, H. D., and Gruber, N.: Continental-scale enrichment of atmospheric  $^{14}\text{C}$  from  
843 the nuclear power industry: potential impact on the estimation of fossil fuel-derived  $\text{CO}_2$ ,  
844 *Atmos Chem Phys*, 11, 12339–12349, doi:10.5194/acp-11-12339-2011, 2011.
- 845 Graven, H. D., Guilderson, T. P. and Keeling, R. F.: Observations of radiocarbon in  $\text{CO}_2$   
846 at La Jolla, California, USA 1992–2007: Analysis of the long-term trend, *J Geophys Res*,  
847 117, D02302, doi:10.1029/2011JD016533, 2012.
- 848 [Graven, H., Xu, X., Guilderson, T. P., and Keeling R. F.: \(2013\), Comparison of](#)  
849 [independent  \$\Delta^{14}\text{C}\$  records at Point Barrow, Alaska, \*Radiocarbon\*, 55, 1541–1545,](#)  
850 [2013.](#)
- 851 Gurney, K. R., I. Razlivanov, Y. Song, Y. Zhou, B. Benes, and M. Abdul-Massin:  
852 Quantification of fossil fuel  $\text{CO}_2$  emissions on the building/street scale for a large U.S.  
853 city, *Environ Sci Technol*, 46, 12194–12202, dx.doi.org/10.1021/es3011282, 2012.
- 854 Gurney, K. R., Romero-Lankao, P., Seto, K. C., Hutyra, L. R., Duren, R., Kennedy, C.,  
855 Grimm, N. B., Ehleringer, J. R., Marcutuillio, P., Hughes, S., Pincetl, S., Chester, M. V.,  
856 Runfola, D. M., Feddema, J. J., and Sperling, J.: Climate change: Track urban emissions  
857 on a human scale, *Nature*, 525, 179–181, doi:10.1038/525179a, 2015.
- 858 Huang, N., Shen, Z. and Long, S.: The empirical mode decomposition and the Hilbert  
859 spectrum for nonlinear and non-stationary time series analysis, *Proc Royal Society*  
860 *London Series A*, 454, 903–995, 1998.
- 861 IEA: World Energy Outlook 2008, edited by: F. Birol, International Energy Agency.  
862 2008.
- 863 IPCC: Climate Change 2013: The Physical Science Basis. Contribution of Working  
864 Group I to the Fifth Assessment Report of the Intergovernmental Panel on Climate  
865 Change [Stocker, T.F., D. Qin, G.-K. Plattner, M. Tignor, S.K. Allen, J. Boschung, A.

Sally Newman 2/22/2016 12:59 PM

**Deleted:** Gonfiantini, R.: Standards for stable isotope measurements in natural compounds, *Nature*, 271, 534–536 [online] Available from: <http://www.nature.com/nature/journal/v271/n5645/pdf/271534a0.pdf> (Accessed 12 October 2012), 1978. .

- 873 Nauels, Y. Xia, V. Bex and P.M. Midgley (eds.]. Cambridge University Press,  
874 Cambridge, United Kingdom and New York, NY, USA, 1535 pp., 2013.
- 875 Jacobson, M. Z.: On the causal link between carbon dioxide and air pollution mortality,  
876 *Geophys Res Lett*, 35, L03809, doi:10.1029/2007GL031101, 2008.
- 877 Jiang, X., Li, Q., Liang, M.-C., Shia, R.-L., Chahine, M. T., Olsen, E. T., Chen, L. L. and  
878 Yung, Y. L.: Simulation of upper tropospheric CO<sub>2</sub> from chemistry and transport models,  
879 *Global Biogeochem. Cy.*, 22, GB4025, doi:10.1029/2007GB003049, 2008.
- 880 Jiang, X., Chahine, M. T., Li, Q., Liang, M., Olsen, E. T., Chen, L. L., Wang, J. and  
881 Yung, Y. L.: CO<sub>2</sub> semiannual oscillation in the middle troposphere and at the surface,  
882 *Global Biogeochem. Cy.*, 26, GB3006, doi:10.1029/2011GB004118, 2012.
- 883 Keeling, C.: The concentration and isotopic abundances of carbon dioxide in rural and  
884 marine air, *Geochim Cosmochim Acta*, 24, 277–298, 1961.
- 885 Keeling, C. D.: The concentration and isotopic abundances of atmospheric carbon  
886 dioxide in rural areas, *Geochim Cosmochim Acta*, 13(4), 322–334, doi:10.1016/0016-  
887 7037(58)90033-4, 1958.
- 888 Kobayashi-Kirschvink, K. J., Li, K.-F., Shia, R.-L., and Yung, Y. L., Fundamental modes  
889 of atmospheric CFC-11 from empirical mode decomposition, *Adv Adapt Data Anal*,  
890 04(04), 1250024, doi:10.1142/S1793536912500240, 2012.
- 891 Kort, E. A., Angevine, W., Duren, R., Miller, C. E.: Surface observations for monitoring  
892 urban fossil fuel CO<sub>2</sub> emissions: minimum site location requirements for the Los Angeles  
893 megacity, *J Geophys Res*, 118, 1-8, doi: 10.1002/jgrd.50135, 2013.
- 894 Levin, I. and Roedenbeck, C.: Can the envisaged reductions of fossil fuel CO<sub>2</sub> emissions  
895 be detected by atmospheric observations?, *Naturwissenschaften*, 95, 203–208,  
896 doi:10.1007/s00114-007-0313-4, 2008.
- 897 Levin, I., Kromer, B., Schmidt, M. and Sartorius, H.: A novel approach for independent  
898 budgeting of fossil fuel CO<sub>2</sub> over Europe by <sup>14</sup>CO<sub>2</sub> observations, *Geophys Res Lett*,  
899 30(23), 2194, 2003.
- 900 Lopez, M., Schmidt, M., Delmotte, M., Colomb, A., Gros, V., Janssen, C., Lehman, S. J.,  
901 Mondelain, D., Perrussel, O., Ramonet, M., Xueref-Remy, I. and Bousquet, P.: CO, NO<sub>x</sub>  
902 and <sup>13</sup>CO<sub>2</sub> as tracers for fossil fuel CO<sub>2</sub>: results from a pilot study in Paris during winter  
903 2010, *Atmos Chem Phys*, 13(15), 7343–7358, doi:10.5194/acp-13-7343-2013, 2013.
- 904 Lu, R. and Turco, R.: Air pollutant transport in a coastal environment. Part I: Two-  
905 dimensional simulations of sea-breeze and mountain effects, *Journal of the Atmospheric*  
906 *Sciences*, 51(15), 2285–2308, 1994.
- 907 Lu, R. and Turco, R.: Air pollutant transport in a coastal environment—II. Three-  
908 dimensional simulations over Los Angeles basin, *Atmos Environ*, 29(13), 1499–1518,

- 909 1995.
- 910 Miller, J. and Tans, P.: Calculating isotopic fractionation from atmospheric  
911 measurements at various scales, *Tellus B*, 55, 207–214, 2003.
- 912 Miller, J. B., Lehman, S. J., Montzka, S. A., Sweeney, C., Miller, B. R., Karion, A.,  
913 Wolak, C., Dlugokencky, E. J., Southon, J., Turnbull, J. C. and Tans, P. P.: Linking  
914 emissions of fossil fuel CO<sub>2</sub> and other anthropogenic trace gases using atmospheric  
915 <sup>14</sup>CO<sub>2</sub>, *J Geophys Res*, 117, D08302, doi:10.1029/2011JD017048, 2012.
- 916 [Miller, J., Lehman, S., Wolak, C., Turnbull, J., Dunn, G., Graven, H., Keeling, R., H.](#)  
917 [Meijer, A., Aerts-Bijma, A. T., and Palstra, S. W.: Initial results of an intercomparison of](#)  
918 [AMS-based atmospheric <sup>14</sup>CO<sub>2</sub> measurements, \*Radiocarbon\*, 55, 1475–1483, 2013.](#)
- 919 Moore, J., and Jacobson, A. D.: Seasonally varying contributions to urban CO<sub>2</sub> in the  
920 Chicago, Illinois, USA region: Insights from a high-resolution CO<sub>2</sub> concentration and  
921 δ<sup>13</sup>C record, *Elem Sci Anth*, 3, 000052, doi:10.12952/journal.elementa.000052.s004,  
922 2015.
- 923 NBER, National Bureau of Economic Research: available at:  
924 <http://www.nber.org/cycles/sept2010.html> (last access: September 2010), 2010.
- 925 Newman, S., Xu, X., Affek, H. P., Stolper, E. and Epstein, S.: Changes in mixing ratio  
926 and isotopic composition of CO<sub>2</sub> in urban air from the Los Angeles basin, California,  
927 between 1972 and 2003, *J Geophys Res-Atmos*, 113, D23304,  
928 doi:10.1029/2008JD009999, 2008.
- 929 Newman, S., Jeong, S., Fischer, M. L., Xu, X., Haman, C. L., Lefer, B., Alvarez, S.,  
930 Rappenglueck, B., Kort, E. A., Andrews, A. E., Peischl, J., Gurney, K. R., Miller, C. E.  
931 and Yung, Y. L.: Diurnal tracking of anthropogenic CO<sub>2</sub> emissions in the Los Angeles  
932 basin megacity during spring 2010, *Atmos Chem Phys*, 13(8), 4359–4372,  
933 doi:10.5194/acp-13-4359-2013, 2013.
- 934 NRC, National Research Council: *Advancing the Science of Climate Change*. National  
935 Research Council. The National Academies Press, Washington, DC, USA, 2010.
- 936 Pataki, D., Bowling, D. and Ehleringer, J.: Seasonal cycle of carbon dioxide and its  
937 isotopic composition in an urban atmosphere: Anthropogenic and biogenic effects, *J*  
938 *Geophys Res*, 108, 4735, 2003.
- 939 Patarasuk, R., Gurney, K. R., O’Keeffe, D., Song, Y., Huang, J., Rao, P., Buchert, M.,  
940 Lin, J., Mendoza, D., and Ehleringer, J.: High-resolution fossil fuel CO<sub>2</sub> emissions  
941 quantification and application to urban climate policy, *Urban Ecosys*, in preparation,  
942 2015.
- 943 Peters, G., Marland, G., Le Quéré, C. and Boden, T.: Rapid growth in CO<sub>2</sub> emissions  
944 after the 2008-2009 global financial crisis, *Nature Climate Change*, 2, 2-4, 2012.

945 Prinn, R. G., Weiss, R. F., Fraser, P. J., Simmonds, P. G., Cunnold, D. M., Alyea, F. N.,  
946 O'Doherty, S., Salameh, P., Miller, B. R., Huang, J., Wang, R., Hartley, D. E., Harth, C.,  
947 Steele, L. P., Sturrock, G., Midgley, P. M. and McCulloch, A.: A history of chemically  
948 and radiatively important gases in air deduced from ALE/GAGE/AGAGE, *J Geophys*  
949 *Res-Atmos*, 105(D14), 17751–17792, doi:10.1029/2000JD900141, 2000.

950 Rao, P., Gurney, K. R., Patarasuk, R., Song, Y., Miller, C. E., Duren, R. M. Duren, and  
951 Eldering, A.: Spatio-temporal variations in onroad vehicle fossil fuel CO<sub>2</sub> emissions in  
952 Los Angeles megacity, *Environ. Sci. Technol.*, submitted, 2015.

953 Rolph, G.D. Real-time Environmental Applications and Display sYstem (READY)  
954 Website: available at: <http://www.ready.noaa.gov> (last access: July 2015), NOAA Air  
955 Resources Laboratory, College Park, MD, 2014.

956 Tans, P. P., Berry, J. A. and Keeling, R. F.: Oceanic 13C/ 12C observations: A new  
957 window on ocean CO<sub>2</sub> uptake, *Global Biogeochem Cycles*, 7(2), 353–368,  
958 doi:10.1029/93GB00053, 1993.

959 Thoning, K., Tans, P. and Komhyr, W.: Atmospheric carbon dioxide at Mauna Loa  
960 Observatory, 2. Analysis of the NOAA/GMCC data, 1974-1985, *J Geophys Res*, 94(D6),  
961 8549–8565, 1989.

962 Turnbull, J., Miller, J., Lehman, S., Tans, P., Sparks, R. and Southon, J.: Comparison of  
963 <sup>14</sup>CO<sub>2</sub>, CO, and SF<sub>6</sub> as tracers for recently added fossil fuel CO<sub>2</sub> in the atmosphere and  
964 implications for biological CO<sub>2</sub> exchange, *Geophys Res Lett*, 33, L01817,  
965 doi:10.1029/2005GL024213, 2006.

966 Turnbull, J., Rayner, P., Miller, J., Naegler, T., Ciais, P. and Cozic, A.: On the use of  
967 (CO<sub>2</sub>)-C-14 as a tracer for fossil fuel CO<sub>2</sub>: Quantifying uncertainties using an  
968 atmospheric transport model, *J Geophys Res-Atmos*, 114, D22302,  
969 doi:10.1029/2009JD012308, 2009.

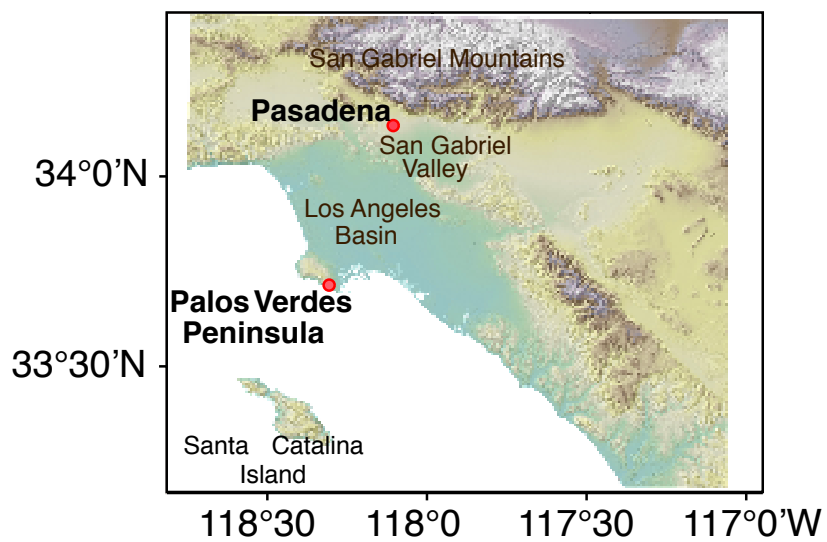
970 Turnbull, J. C., Karion, A., Fischer, M. L., Faloona, I., Guilderson, T., Lehman, S. J.,  
971 Miller, B. R., Miller, J. B., Montzka, S., Sherwood, T., Saripalli, S., Sweeney, C. and  
972 Tans, P. P.: Assessment of fossil fuel carbon dioxide and other anthropogenic trace gas  
973 emissions from airborne measurements over Sacramento, California in spring 2009,  
974 *Atmos Chem Phys*, 11(2), 705–721, doi:10.5194/acp-11-705-2011, 2011.

975 Turnbull, J. C., Sweeney, C., Karion, A., Newberger, T., Lehman, S. J., Tans, P. P.,  
976 Davis, K. J., Lauvaux, T., Miles, N. L., Richardson, S. J., Cambaliza, M. O., Shepson, P.  
977 B., Gurney, K., Patarasuk, R. and Razlivanov, I.: Toward quantification and source sector  
978 identification of fossil fuel CO<sub>2</sub> emissions from an urban area: Results from the INFLUX  
979 experiment, *J Geophys Res-Atmos*, 120, 292–312, doi:10.1002/2014JD022555, 2015.

980 Vardag, S. N., C. Gerbig, G. Janssens-Maenhout, and I. Levin: Estimation of continuous  
981 anthropogenic CO<sub>2</sub> using CO<sub>2</sub>, CO, δ<sup>13</sup>C(CO<sub>2</sub>) and Δ<sup>14</sup>C(CO<sub>2</sub>), *Atmos. Chem. Phys.*  
982 *Discuss.*, 15(14), 20181–20243, doi:10.5194/acpd-15-20181-2015, 2015.

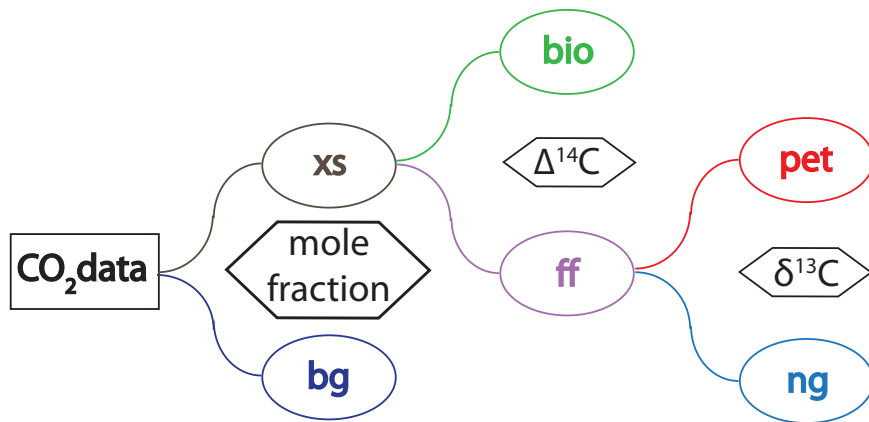
- 983 Widory, D. and Javoy, M.: The carbon isotope composition of atmospheric CO<sub>2</sub> in Paris,  
984 Earth Planet Sci Lett, 215(1-2), 289–298, 2003.
- 985 Wong, K. W., Fu, D., Pongetti, T. J., Newman, S., Kort, E. A., Duren, R., Hsu, Y.-K.,  
986 Miller, C. E., Yung, Y. L., and Sander, S. P.: Mapping CH<sub>4</sub>:CO<sub>2</sub> ratio in Los Angeles  
987 with CLARS-FTS from Mount Wilson, Atmos Chem Phys, 15, 241-252, 2015.
- 988 World Bank: GDP,  
989 [http://data.worldbank.org/indicator/NY.GDP.MKTP.CD/countries/1W-US?](http://data.worldbank.org/indicator/NY.GDP.MKTP.CD/countries/1W-US?display=graph)  
990 [display=graph](http://data.worldbank.org/indicator/NY.GDP.MKTP.CD/countries/1W-US?display=graph), last access: May 2015.
- 991 Wu, Z. and Huang, N. E.: Ensemble empirical mode decomposition: A noise-assisted  
992 data analysis method, Adv Adapt Data Anal, 1(01), 1–41, 2009.
- 993 Xu, X., Trumbore, S. E., Zheng, S., Southon, J. R., McDuffee, K. E., Luttgen, M. and  
994 Liu, J. C.: Modifying a sealed tube zinc reduction method for preparation of AMS  
995 graphite targets: Reducing background and attaining high precision, Nucl Instrum Meth  
996 B, 259, 320–329, 2007.
- 997 [Xu, X., Khosh, M. S., Druffel-Rodriguez, K. C., Trumbore S. E., and Southon J. R.:](#)  
998 [\(2010\). Is the consensus value of ANU sucrose \(IAEA C-6\) too high? Radiocarbon, 52,](#)  
999 [866-874, 2010.](#)
- 1000 York, R.: Asymmetric effects of economic growth and decline on CO<sub>2</sub> emissions, Nature  
1001 Climate Change, 2(11), 762–764, doi:10.1038/nclimate1699, 2012.

1002 FIGURES

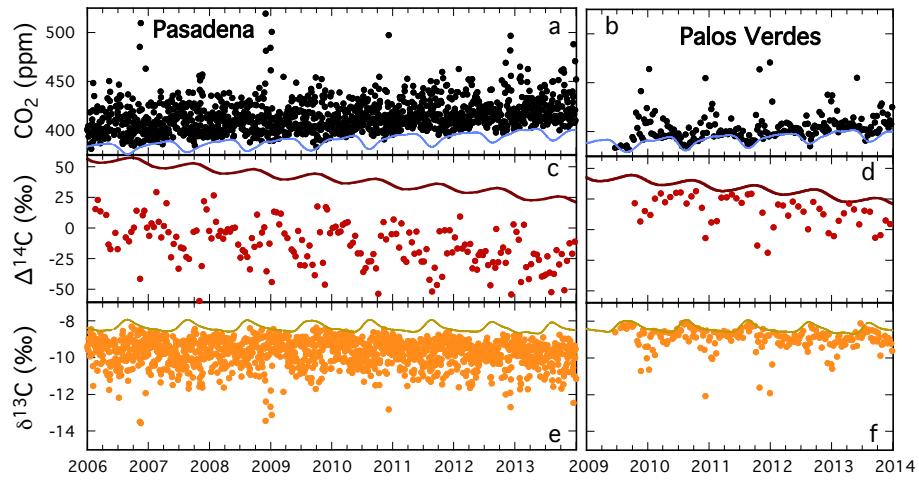


1003 Figure 1. Map of southern California, showing sampling locations in Pasadena and Palos  
1004 Verdes (red dots).

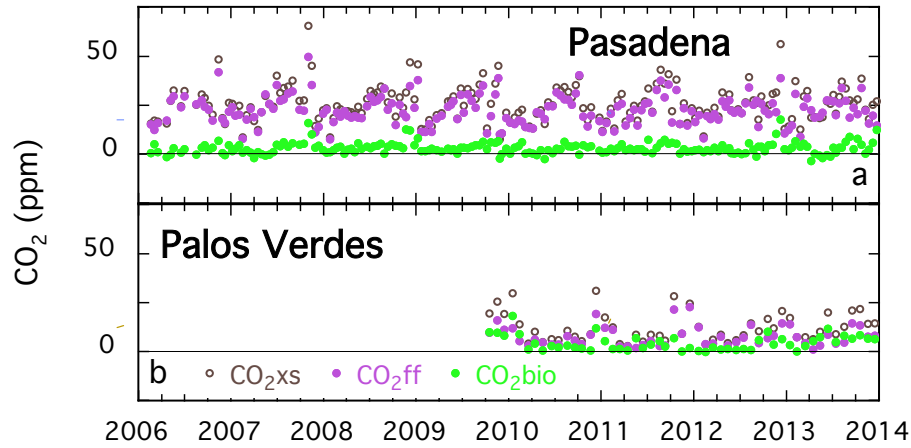




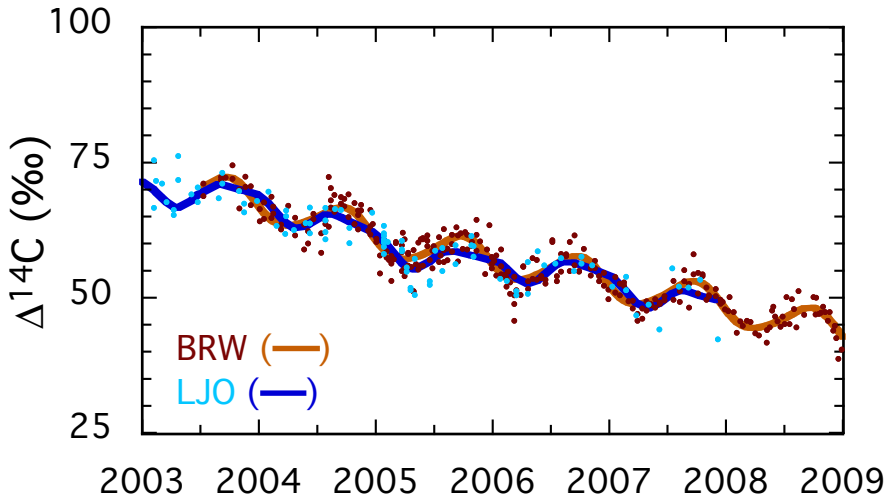
1005 Figure 2. Schematic diagram showing the use of different data sets for attribution of the  
 1006 sources of CO<sub>2</sub> emissions. Mole fractions of background (bg) and observations are used  
 1007 to determine C<sub>xs</sub> (excess over background/bg); Δ<sup>14</sup>C values are used to distinguish C<sub>ff</sub>  
 1008 (fossil fuel, ff) and C<sub>bio</sub> (biosphere, bio); δ<sup>13</sup>C compositions are used to distinguish C<sub>pet</sub>  
 1009 (petroleum/gasoline, pet) from C<sub>ng</sub> (natural gas, ng).



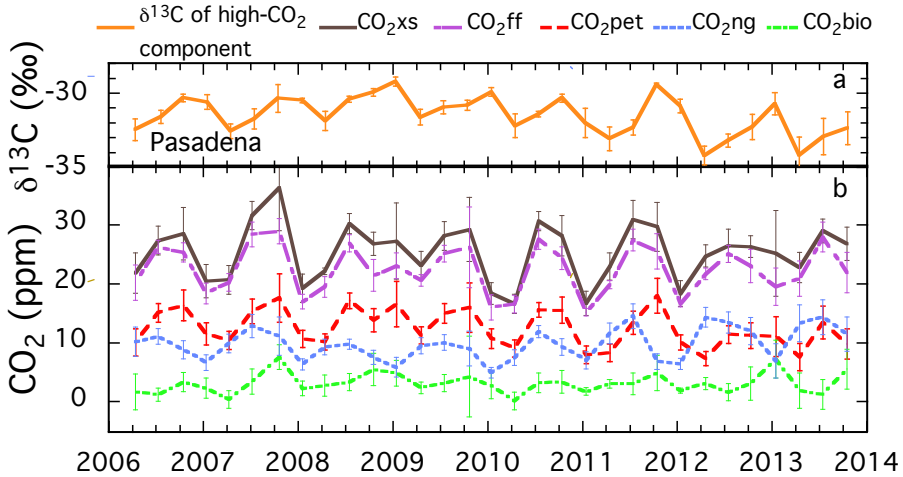
1010 Figure 3. Time series of CO<sub>2</sub> mole fractions for <sup>14</sup>CO<sub>2</sub> samples (a, b), Δ<sup>14</sup>C data (c, d),  
 1011 and δ<sup>13</sup>C (e, f) for Pasadena and Palos Verdes. The solid curves are backgrounds used in  
 1012 the calculations: δ<sup>13</sup>C and CO<sub>2</sub> backgrounds are from La Jolla, CA and Δ<sup>14</sup>C from Pt.  
 1013 Barrow, AK.



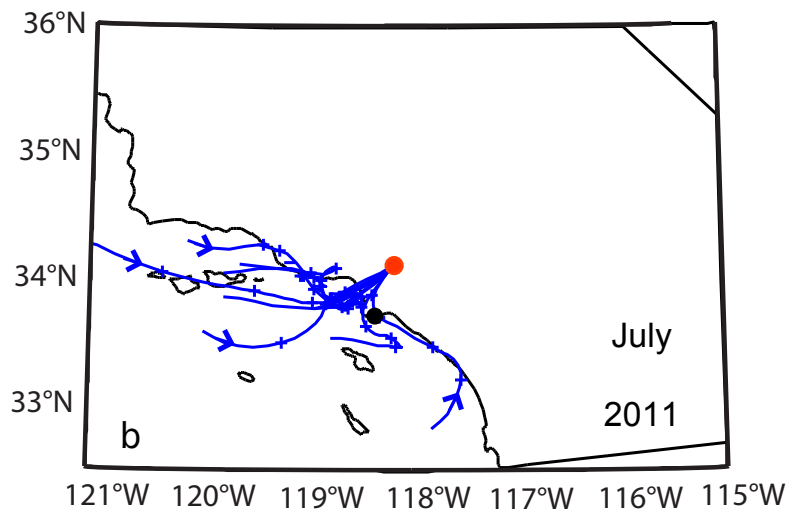
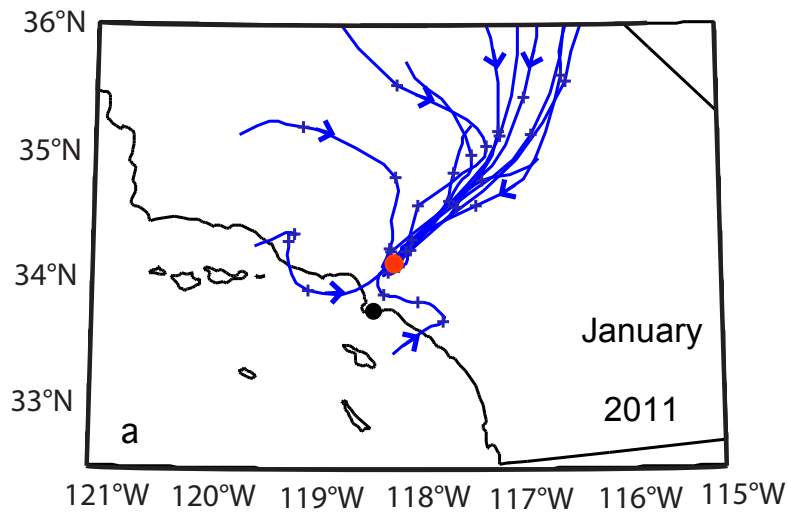
1014 Figure 4. Time series of  $C_{xs}$ ,  $C_{ff}$ , and  $C_{bio}$  calculated from  $\Delta^{14}C$  (see text for description of  
 1015 calculations) for Pasadena (a) and Palos Verdes (b). The errors for  $C_{ff}$  are 1 ppm. The  
 1016 negative  $C_{bio}$  values indicate photosynthetic uptake. The value of  $\Delta^{14}C$  for fuel for this  
 1017 calculation was taken to be -954 ‰, the average from the summer and winter  
 1018 calculations.



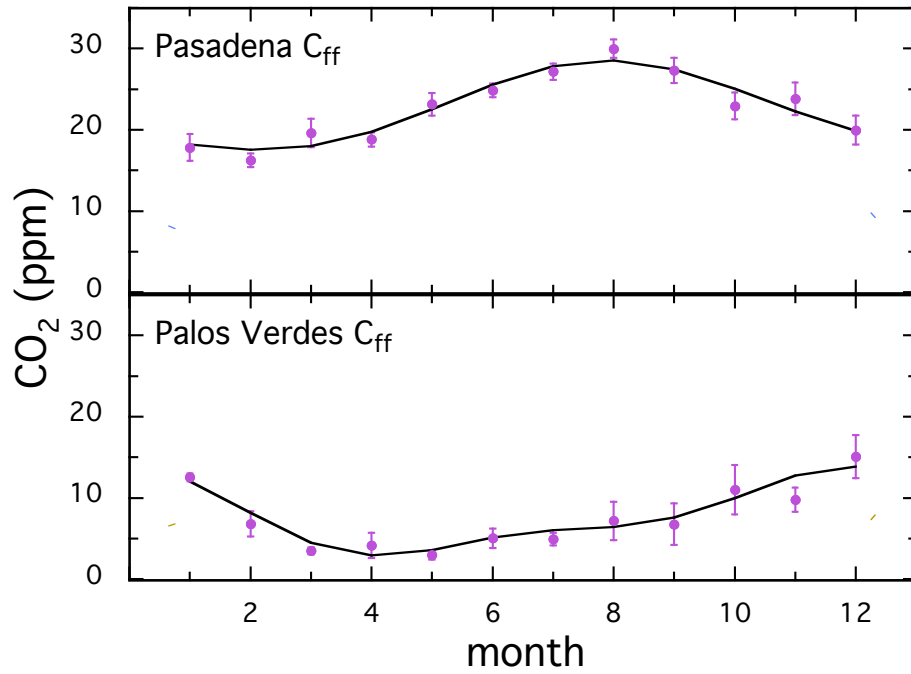
1019 Figure 5. Comparison of possible background records for this study, Pt. Barrow, AK,  
 1020 (BRW; Xiaomei Xu, unpublished data) and La Jolla, CA (LJO; Graven et al., 2012). The  
 1021 smoothed brown curve for BRW is the  $\Delta^{14}\text{C}$  background used for this study and was  
 1022 calculated using the algorithm of Thoning et al. (1989), from the function plus the  
 1023 smoothed residuals of the long-term trend, using 2 harmonic and 3 polynomial terms in  
 1024 the function and 667 days as the long-term cutoff for the low-pass filter.



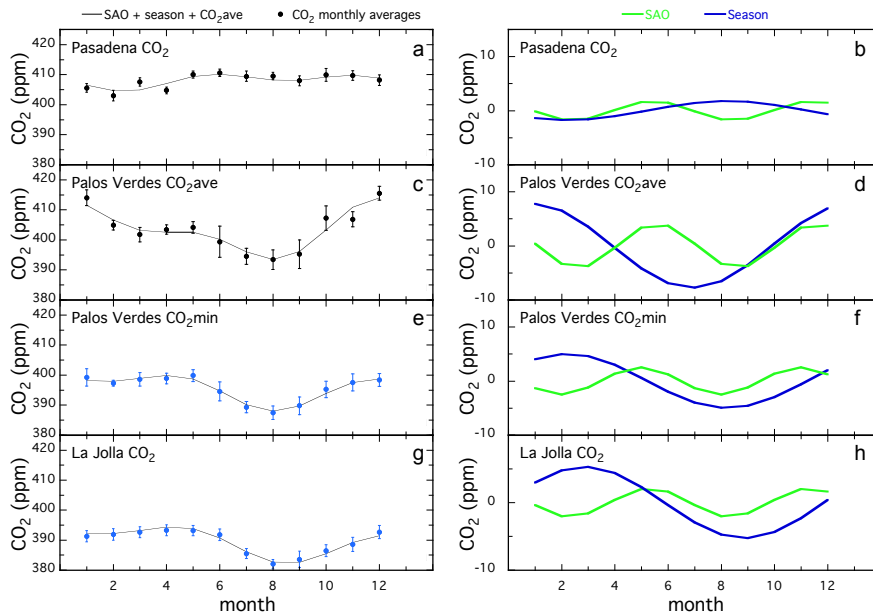
1025 Figure 6. Attribution of CO<sub>2</sub> excess in Pasadena among combustion of natural gas and  
 1026 petroleum and the biosphere. (a) Miller-Tans slopes for seasonal averages of monthly  
 1027 plots. Error bars are standard errors of the regression intercepts. (b) Attribution of C<sub>xs</sub>  
 1028 among all three sources (natural gas, petroleum, and the biosphere), combining the  
 1029 information from Δ<sup>14</sup>C and δ<sup>13</sup>C, using Miller-Tans slopes to determine the relative  
 1030 proportions of petroleum and natural gas combustion. Error bars are propagated from the  
 1031 errors in the δ<sup>13</sup>C intercepts and the Δ<sup>14</sup>C measurements.



1032 Figure 7. Back trajectories (24 hour) for winds arriving at the Pasadena site (red dot) at  
 1033 1400 PST for January (a) and July (b) 2011, calculated by HYSPLIT (Draxler and Rolph,  
 1034 2015; Rolph, 2015) for all sampling days in January and selected sampling days in July,  
 1035 for clarity. Results for all sampling days are shown in Fig. A2. Arrows indicate the  
 1036 direction of air flow. Plus signs indicate 6, 12, and 18 hours from the Pasadena site. The  
 1037 back trajectories for the Palos  
 1038 Verdes site show a similar pattern (Appendix Fig. A2). The back trajectories explain the  
 1039 difference between the annual cycles at the two sites, shown in Fig. 8.

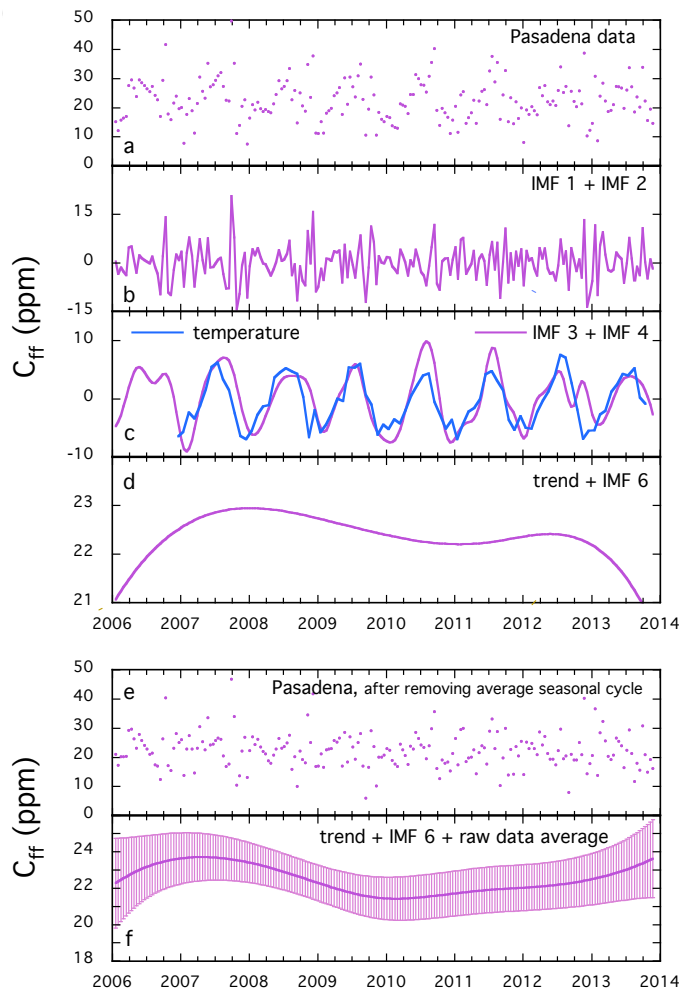


1040 Figure 8. The annual patterns for  $C_{ff}$  in Pasadena and Palos Verdes calculated as the best  
 1041 fit of two harmonics plus the average of the annual cycles (black curves). These patterns  
 1042 are consistent with seasonal differences in the back trajectories shown in Fig. 7.



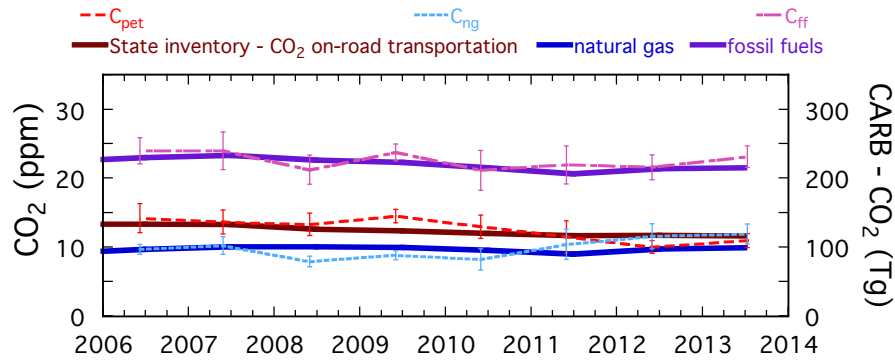
1043 Figure 9. Comparison of seasonal and semi-annual oscillation cycles of CO<sub>2</sub> mole  
 1044 fractions for flask samples from Pasadena (2006-2013) with those at the La Jolla (2006-  
 1045 2013) and Palos Verdes (2009-2013) sites. Left column panels show the average annual  
 1046 patterns for the monthly averages together with the sum of the harmonics for seasonal  
 1047 (blue) and semi-annual (green) cycles (Jiang et al., 2008). Right column panels show the  
 1048 amplitudes and phases of the pure harmonic components. Two sets of results are shown  
 1049 for Palos Verdes, for the monthly averages (c, d) and for the monthly averages of weekly  
 1050 minima (e, f). The monthly averages show the effect of transport on the signal, with a  
 1051 large peak during the winter, while the minima (in blue) show that data from this site are  
 1052 very similar to La Jolla (in blue) and should be a good estimation of the background air  
 1053 for the LA basin. Error bars on the monthly averages of the data are  $1\sigma$  standard errors.



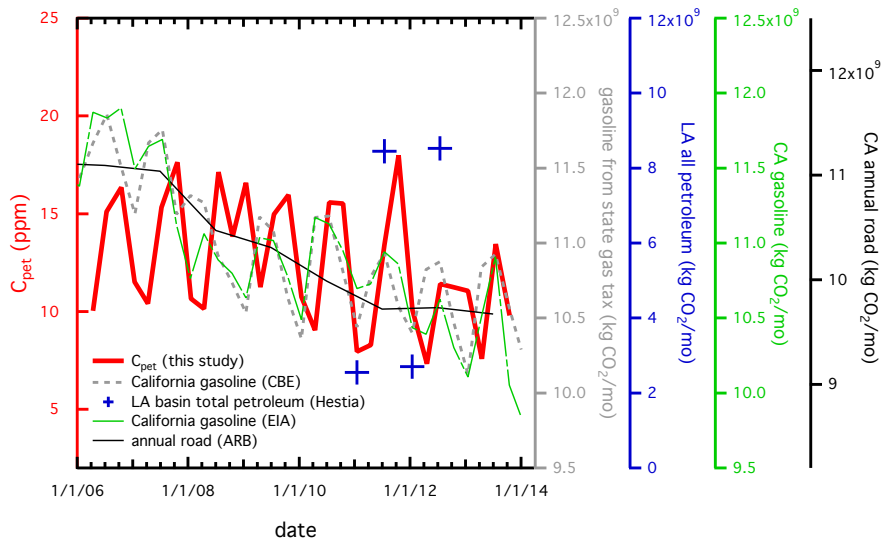


1054 | Figure 10. Results of ensemble empirical mode decomposition (EEMD) (Huang et al.,  
 1055 | 1998; Wu and Huang, 2009) of the  $C_{ff}$  time series calculated using Eq. (3) and the  
 1056 | average, constant  $\Delta^{14}C$  of  $-954\text{‰}$  for fossil fuel. The top set of panels show the raw data  
 1057 | (a), noise (b), annual and semi-annual mode (c), and the trend + IMF 6 (d). The pattern  
 1058 | of the trend + IMF 6 shown in (d) is within  $1\sigma$  uncertainty of no variation over this time  
 1059 | period. The bottom two panels include the raw data after subtracting the average annual  
 1060 | cycle (centered at zero) (e) and the trend + IMF 6 for the modified data set (f). 30-day  
 1061 | average temperatures (minus the overall average and scaled to match the magnitude of  
 1062 | the  $C_{ff}$  IMF; blue curve) are superimposed on the plot of IMF 3 + IMF 4 (c). Shaded  
 1063 | regions in (f) indicate  $1\sigma$  standard deviation of 300 Monte Carlo realizations with 13.7 %  
 1064 | noise added, the ratio of the uncertainty in  $C_{ff}$  to the standard deviation of the data.

Unknown  
 Formatted: Font:Times, Bold

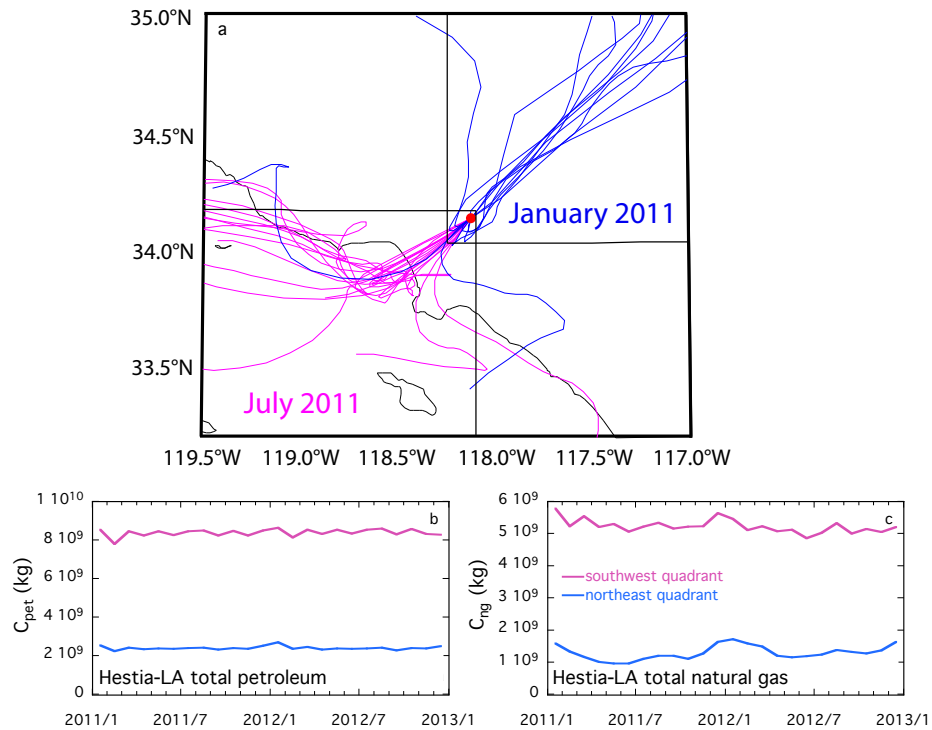


1065 Figure 11. Comparison of annual average CO<sub>2</sub> emissions from bottom-up California Air  
 1066 Resources Board (CARB) inventories (thick lines; right axis labels) for fossil fuel-  
 1067 derived emissions with top-down annual averages from the Pasadena data, using the  
 1068 Miller and Tans (2003) approach to attribute CO<sub>2</sub> emissions from petroleum and natural  
 1069 gas combustion from the  $\delta^{13}\text{C}$  measurements. Annual curves showing the attribution of  
 1070  $C_{\text{xs}}$  averaged from the seasonal values from Fig. 6b are shown as thinner lines. The error  
 1071 bars on the results from the flask sample data are  $1\sigma$  standard errors of the means. The  
 1072 annual trends from the bottom-up CARB inventories are plotted on a scale exactly 100  
 1073 times that of the trends derived from the CO<sub>2</sub> measurements, showing that the relative  
 1074 proportions are very similar through 2013.

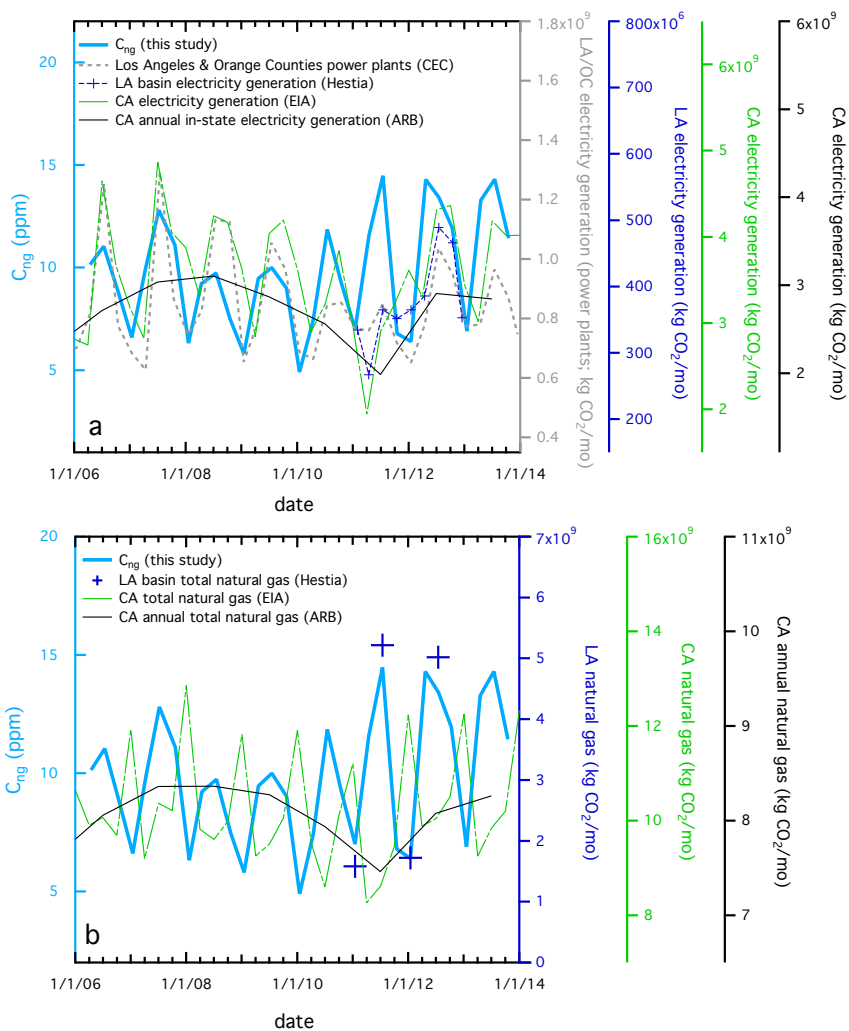


1075 Figure 12. Comparison of the Pasadena  $C_{pet}$  atmospheric concentration with all available  
 1076 area-integrated bottom-up fossil fuel  $CO_2$  emissions **per month (mo)**, including gasoline  
 1077 sales based on taxes paid to the California Board of Equalization (CBE, 2014), gasoline  
 1078 provided in California by prime suppliers, the California Air Resources Board's annual  
 1079 road emissions (CARB, 2015), and the Hestia-LA gridded total petroleum. The Hestia-  
 1080 LA data product is specific to the Los Angeles megacity domain; all inventories are  
 1081 statewide estimates. Since the Hestia-LA product is gridded, we show the emissions  
 1082 emanating from different regions for January (northeast quadrant, Fig. 13a) and July  
 1083 (southwest quadrant), based on prevailing winds during those periods (Figs. 7 and 13a).  
 1084 The axis for each inventory has been adjusted to allow easy comparison. The seasonality  
 1085 of the  $C_{pet}$  data lags the bottom-up inventories by a few months. This analysis is  
 1086 consistent with the observed decrease in gasoline combustion during 2008-2011.

Unknown  
 Formatted: Font:(Default) Times New Roman

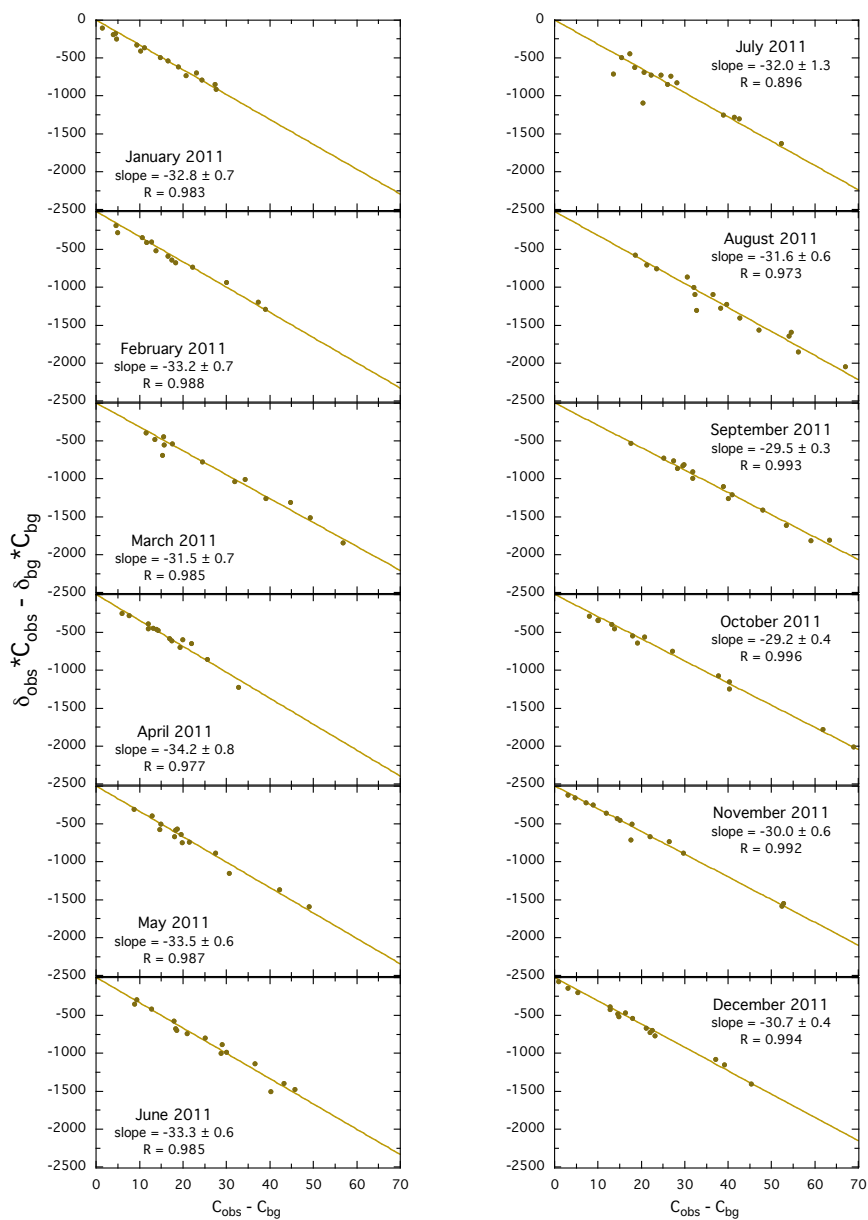


1087 Figure 13. Relevant emissions selection from the Hestia-LA data product. (a) Quadrants  
 1088 selected for investigation of CO<sub>2</sub> emissions from the Hestia-LA data product, together  
 1089 with the 24-hour back trajectories calculated by HYSPLIT for January (northeast  
 1090 quadrant) and July (southwest quadrant)  $\Delta^{14}\text{C}$  sampling days. The back trajectories end  
 1091 in Pasadena (red dot) at 1400 PST. Monthly averaged time series for Hestia-LA data  
 1092 product  $C_{\text{fi}}$  are shown from total petroleum combustion (b) and total natural gas  
 1093 combustion (c) for 2011 and 2012. For both the northeast quadrant of the Los Angeles  
 1094 region, the source of winter emissions, and the southwest quadrant, the source of summer  
 1095 emissions, the seasonal pattern is either flat (petroleum) or characterized by peaks during  
 1096 the winter (natural gas). But the summer emissions are always higher than those during  
 1097 winter, consistent with the observed top-down patterns for  $C_{\text{pet}}$  and  $C_{\text{ng}}$  in Pasadena.



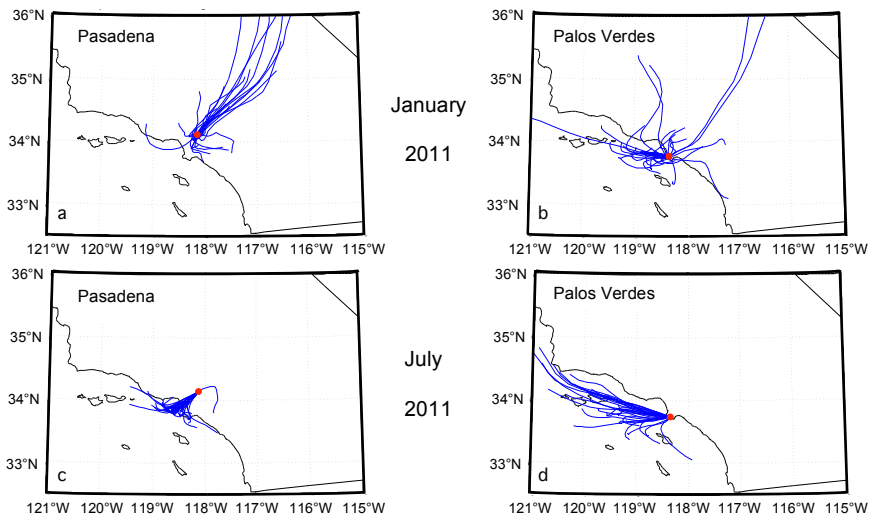
1098 Figure 14. Comparison of Pasadena  $C_{ng}$  atmospheric concentration with area-integrated  
 1099 inventories of natural gas combustion, as well as the gridded Hestia-LA data product for  
 1100 southwest and northeast regional sectors for July and January months, respectively, in  
 1101 emissions/month (mo). Panel (a) compares the data from this paper with usage of natural  
 1102 gas by the electrical power sector; panel (b) shows the comparison with total natural gas  
 1103 consumption. Statewide inventories are given by EIA (2014) and CARB (2015) curves.  
 1104 Regional inventories include Hestia results and natural gas from power plants (CEC,  
 1105 2014) in Los Angeles and Orange counties with monthly data (except Calabasas and  
 1106 Valencia). The vertical axes have been adjusted to allow easy comparison. This analysis  
 1107 is consistent with the increase in natural gas usage during the last few years.

1108 Appendix  
 1109 1. Monthly Miller Tans plots for 2011



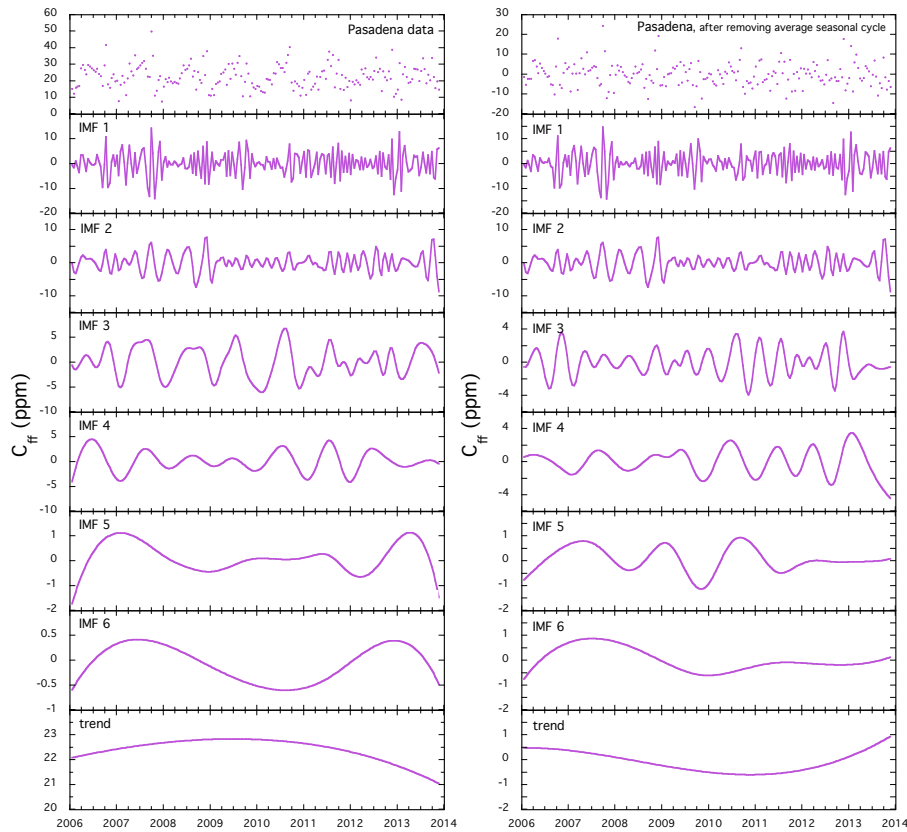
1110 Figure A1. Miller-Tans plots for each month in 2011. Values of the slopes for three-  
 1111 month seasonal averages are plotted in Fig. 6a.

1112 2. Back trajectories for both Pasadena and Palos Verdes sites



1113 Figure A2. Twelve-hour back trajectories for all days in January and July, 2011, for the  
1114 Pasadena and Palos Verdes sites. This shows more detail for the effect of transport on the  
1115 air masses sampled during summer and winter at the Palos Verdes site than Fig. 7.

1116 **3. Full ensemble empirical mode decomposition results**



1117 Figure A3. Time series of all of the results from the ensemble empirical mode  
 1118 decomposition (EEMD) analysis of the Pasadena  $C_{ff}$ . The left set of panels shows the  
 1119 results for the raw data, whereas the right column shows those for the data after  
 1120 subtraction of the average seasonal cycle. The long-term trend reflecting the economic  
 1121 downturn of the Great Recession is reflected clearly in IMF 6 and the trend of the data  
 1122 after the pronounced seasonality is removed (right-hand column), although there is some  
 1123 evidence of it in IMF 6 of the raw  $C_{ff}$  data.



Responses for Referee #1's comments:

Abstract, p. 29593 1.23 The absolute agreement between the bottom up Hestia and top-down approach is not assessed. Therefore, the word "consistent" may be misleading. At some latter point in the manuscript it may be worthwhile to clearly state that emission inventories are not validated absolutely, but only trends (and relative contributions) of bottom-up and top-down approaches are compared.

We have made a minor modification in the title to clarify that this study compares trends in emissions between top-down atmospheric data and bottom-up inventories and data products, not the absolute emissions. The title is now:

Toward consistency between trends in bottom-up CO<sub>2</sub> emissions and top-down atmospheric measurements in the Los Angeles megacity

In the abstract, only variations, seasonality, and trends are discussed. Hopefully, the change in the title will clarify the focus.

p. 29597 1.12 The PDB scale has long been replaced by the VPDB scale and it is recommended to use the VPDB scale.

Thank you for finding this error. It has been corrected, both in the text and in the references.

p. 29597 1.14-17 In this study, an integrated 14C(CO<sub>2</sub>) sample is obtained by combining 3-7 CO<sub>2</sub> samples (afternoon) into one sample. Thus, 14C(CO<sub>2</sub>) from this integrated sample provides the average fossil fuel CO<sub>2</sub> offset. In this manuscript, the monthly-integrated source signature  $\delta_{ss}$  is used to obtain a value for  $\delta_{ff}$ . However, averaging the source signature  $\delta_{ff}$  over time is only valid if  $\delta_{ff}$  and  $\delta_{bio}$  do not change over time as otherwise correlation between  $\delta_{ff}$  and  $\delta_{ff}$  and  $\delta_{bio}$  and  $\delta_{bio}$  can lead to biases (Vardag et al., 2015). As the CO<sub>2</sub> samples are always taken during the same (short) time of the day and the integration period is not long, it may be that the effect of the integration is small. However, it might be worthwhile to check and mention this in the manuscript.

This is an interesting point. The Miller-Tans plots suggest that monthly average compositions for  $\delta_{xs}$  are constant, within uncertainty, as indicated by the very high correlation coefficients (Fig. A1). Although this does not guarantee that  $\delta_{ff}$  and  $\delta_{bio}$  do not change over time, it does suggest that the system is stable over this time scale. A comment has been added to this effect in Section 2.3.3.

p. 29599 1.20 Please give information on the background  $\Delta^{14}C$  values such as sampling resolution, precision etc.

The background  $\Delta^{14}C$  record at Pt. Barrow, AK is obtained through the UCI/NOAA ESRL (Earth System Research Laboratory) flask network program that collects whole air samples using 6-L, 1-valve stainless steel canisters (Silco Can, Restek Co.) that have been pre-evacuated at UCI. The canisters are pressurized to ~2 atm using an oil-free pump. Two biweekly samples were collected before 2008, and one weekly afterwards. For the period from 17 June 2005 to 17 March 2006, some duplicate samples were collected using 32-L, 1-valve stainless steel canisters. Subsamples were then taken from these samples for <sup>14</sup>C analysis. CO<sub>2</sub> is extracted cryogenically at UCI

then converted to graphite by the sealed tube zinc reduction method (Xu et al. 2007). Each sample is ~2.7 mg C in size. Analysis of  $\Delta^{14}\text{C}$  is performed at the W M Keck AMS facility at UCI with total measurement uncertainty of  $\pm 1.3\text{--}2.4\%$ . Mass dependent fractionation is corrected for using “on-line”  $\delta^{13}\text{C}$  measurements during AMS analysis, which accounts for fractionation that occurred during graphitization and inside the AMS.

Comparison was made over 22 common sample dates spanning 5 yr, differences in measured  $\Delta^{14}\text{C}$  from Barrow between the UCI and the Scripps Institution of Oceanography’s  $\text{CO}_2$  Program. It shows differences in measured  $\Delta^{14}\text{C}$  are consistent with the reported uncertainties and there is no significant bias between the programs (Graven et al., 2013).

The other is the inter-comparison of AMS-based atmospheric  $^{14}\text{CO}_2$  measurements organized by the NOAA Earth System Research Laboratory, Boulder, Colorado. UCI lab is one the three groups having interlaboratory comparability within 1‰ for ambient level  $^{14}\text{CO}_2$  (Miller et al. 2013).

This information has been added to Section 2.3.2.

p. 29601 Section 2.3.3. The samples used were all taken during the afternoon hours. However, Miller and Tans (2003) have pointed out that the determination of source signature does not work when  $\text{CO}_2$  sinks with a different signature than the sources occur. If this is the case in your setting, it may lead to potential biases of the source signature, which should be discussed here.

There are minimal, if any, sinks for  $\text{CO}_2$  in this region. The biosphere, as indicated by our data, is not an important player, in general.

p. 29602 1.11 The authors use  $\delta_{\text{bio}}$  of -26.6,  $\delta_{\text{ng}}$  of -40.2 and  $\delta_{\text{pet}}$  of -25.5 without stating an uncertainty or typical variation within one year. It should be elaborated how these uncertainties (especially on a seasonal scale) influence the results for cff, cbio, cpet and cng. This should also be included in Fig. 3.

We do not have a measure of the uncertainty for  $\delta_{\text{bio}}$ , although the sensitivity studies of Bakwin et al. (1998) suggest little variation. However, we have analyzed  $\delta_{\text{ng}}$  and  $\delta_{\text{pet}}$  over many years and at different times of year and the standard deviations are  $\pm 0.5$  and  $1.0\%$ , respectively. We did, in fact, expect a seasonal variation in  $\delta_{\text{pet}}$ , because there are winter and summer blends of gasoline. However, we have observed no significant differences.

p.29606 1.16-22 This section is a bit confusing as the assumption of having no biospheric influence is not correct and also not used in this study. It might be more straightforward to leave this passage out as it seems to be of no use for the reader at this point.

Thank you for pointing this out. This was mentioned above and therefore is redundant here. It has been deleted.

p. 29607 1.5 Throughout the manuscript emission and concentration are used synony-

mously. Without a model, only the contribution of fossil fuel CO<sub>2</sub> can be derived but not the fossil fuel CO<sub>2</sub> emission. Please correct this in the entire manuscript.

Here and in many other places throughout the manuscript fossil fuel “emissions” has been replaced by C<sub>ff</sub>.

p. 29608 1.9 Jiang et al. (2012) concluded that the semi-annual oscillation is a consequence of a combination of gross primary production (GPP) and respiration (resp), not net primary production (NPP=GPP+resp) and respiration.

CO<sub>2</sub> semi-annual oscillation is a consequence of a combination of gross primary production and respiration. We have revised this in the main text.

Fig. 11 It might be worthwhile to insert error bars on cpet and cng.

C<sub>pet</sub> and C<sub>ng</sub> are now shown as annual averages with standard error bars.

p. 29612 1.2 Could the lag be an artifact of not including seasonal variations of the source signatures (e.g. δbio) into the consideration?

We conclude that the major cause of the seasonal variations is the seasonal shift in wind direction, resulting in a different source region for winter versus summer. None of our information suggests seasonal variations in δbio.

Fig. 12 The uncertainty of cpet should be included in this Figure. Why do EIA and ARB statistics differ by a factor 10<sup>3</sup>? Please elaborate what “mo” stands for in the unit of [kg CO<sub>2</sub>/mo]?

We have the uncertainties plotted in Figure 6 and feel that Figure 12 will be too cluttered if they are included here again. Thanks very much for noticing the error of 10<sup>3</sup> in the units for the EIA data. This has been corrected. [kg CO<sub>2</sub>/mo] refers to kg CO<sub>2</sub> per month. This has been added to the caption.

p.29612 1.20 They agree in the direction of the sub-annual variation, but not in their absolute values.

A phrase has been added to say that they agree in their seasonality.

Fig. 14 Same emission sectors should have the same y-scale so that differences between emission inventories become obvious. This is the case for the green and black axes in Fig 14.

The blue axis is for the LA basin Hestia product, covering a much smaller domain, as does the grey axis, which is for LA and Orange county power plant emissions.

The major point being portrayed in this figure is the seasonality. The absolute numbers do not really matter, since the temporal variations are being emphasized.

p.29613 1.6-7 It is interesting that the increase in natural gas consumption is seen earlier in the data than in the emission inventories. If other sectors have not changed significantly (as one might expect?), this might point towards a false emission inventory and might be worth to point out here.

This is a very good point, and we have added a sentence mentioning possible explanations for the different timing. We feel that we cannot suggest a false emission inventory because of the large uncertainties and the lack of atmospheric

modeling here.

p. 29613 1.27 What about long-term changes in source signature of natural gas or petrol? Only if the endmembers of the signature do not change over time it is possible to validate emission inventories as presented here.

We have analyzed natural gas combustion over 30 years and gasoline combustion over 9 years and do not see any significant changes. A comment to this effect has been added in Section 2.3.3.

p. 29615 1.9-14 What are typical uncertainties of the emission inventories used? What are the uncertainties of the top-down approach?

Uncertainties are not given for the bottom-up inventories. We do not produce an emission inventory with our top-down approach. We conclude that we can see a significant 10 % change in  $C_{ff}$  using our measurements.

p. 29638 Fig. A3 Please explain why the long-term trend (last row) changes after removing the average (repeated seasonal cycle).

The major reason for the change in the long-term trend between the analysis of the raw values for  $C_{ff}$  and those after removing the seasonal cycle is that the uncertainties are overwhelming for the raw data analysis and are much smaller after removing seasonality, which is a common artifact of EEMD known as mode mixing between the dominant mode (i.e. annual cycle in our case) with other modes (e.g. noise). In our case, we can minimize the mode-mixing problem by removing the annual cycle and perform EEMD again. The variations observed are not significant for the raw data analysis, whereas they are for the modified data set. In the revised text:

“Note that there are severe mode mixing problems in IMF3 (e.g. during 2011–2013) between the dominant annual cycle and subseasonal variations, which also affects the nonlinear decompositions in the higher modes. To minimize the effects of mode mixing on the extractions of inter-annual trends, we perform the EEMD again after removing the average annual cycle (minus the mean of the raw data), defined as monthly averages over the entire time period (2006-2013; resulting time series shown in Fig. 10e). The revised inter-annual trend is shown in Fig. 10f.”

Technical corrections:

p. 29594 1.13 This is only true in very large cities (Megacities).

We have added the phrase “especially in megacities.”

p. 29595 1.27 It is not clear what “all three” refers to here.

We have added a parenthetical remark to explicitly list “all three sources” for clarification.



Response to Referee Jocelyn Turnbull's comments:

Pg 29594 lines 19-20. Indeed bottom-up reporting may not always be reliable, but this comment should be backed up with references, and perhaps more careful phrasing to avoid the implication of finger pointing at "other" countries.

We have changed the wording and added Andres et al. (2012) as a reference.

Pg 29595 lines 1-3. Are there examples outside of the US? Airparif?

There are no examples of such detailed emissions products outside the US of which we are aware.

Pg 29597 lines 18-22. This is an interesting point – what is the optimal number/time length of samples to combine for measurement to give sensible, useful averages? This could be expanded on here or in the results section.

Since all of our samples were aggregated, we have no way to know the optimal number. We see the difference compared with sparser, individual sampling reported by Affek et al. (2006). This is a good study to do in the future, pending funding.

Pg 29597 line 18. Typo – CCAMS.

Good catch, thank you! This has been changed.

Pg 29597 lines 26-27. The CO<sub>2</sub> mole fraction error is quite large – I would guess that it is sufficient for this study, but this should be justified.

A comment has been added, explaining that the dominant source of error is from the  $\Delta^{14}\text{C}$  analyses.

Pg 29598 line 1. How were the 14C errors determined? Is this described in the Xu 2007 paper? Please reference or describe this.

Overall precision is 2‰ which is based on long-term reproducibility of secondary standards. It is described in both Xu et al. 2007 and Xu et al. 2010 papers. Also see the two inter-lab comparisons in the response to Reviewer #1 above.

Pg 29598 lines 23-24. It is a pity there is no more recent La Jolla 14C data.

We agree completely and eagerly hope for funding to continue the analyses.

Pg 29600, lines 9-10. I take it that the nuclear contribution is therefore ignored?

Yes, we have added a comment to this effect.

Pg 29602, line 11. How was the biosphere discrimination determined? The value appears to assume C<sub>3</sub> plants, but are C<sub>4</sub> plants important in Southern California? Is lawn grass in this area typically C<sub>3</sub> or C<sub>4</sub>? And whether C<sub>3</sub> or C<sub>4</sub>, how certain is this value, and how much seasonal variability might there be? A bias (seasonal or general) in delta-bio would dramatically change the proportions of petroleum and gas determined by this method.

This has been described more thoroughly in the text, in Section 2.3.3. Thank you for raising this important issue. The discussion is as follows:

This value represents data from temperate northern latitudes (28 – 55 °N), dominated

by C3 plants with some C4 grasses present (Bakwin, et al., 1998). Indeed, grasses in southern California are mostly C3 ryes, fescue, and bluegrass, with some C4 grasses such as St. Augustine ([www.cropsreview.com/c3-plants.html](http://www.cropsreview.com/c3-plants.html), last accessed January 25, 2016).

Pg 29603 lines 1-3. This is a reasonably large correction – how large is it relative to the  $C_{bio}$  values themselves? Is what % of  $C_{bio}$  does it represent?

We have added to the text:

The magnitude of this correction is 0.5 – 1.2 ppm, averaging 0.84 ppm, which represents approximately a quarter of the  $C_{bio}$ , but the latter is very small, averaging 3 – 4 ppm and the correction does not affect our results with respect to  $C_{pet}$  and  $C_{ng}$ .

Section 2.3.4 Time series analysis. The description given here is quite brief, and it is hard to follow the results later. This section could be expanded to clarify what the different IMF categories represent, and how they are determined. See also my comment on the IMF results section.

We have added a description of the algorithm to Section 2.3.4.

Pg 29603 line 23. Bottom-up data products, not inventories – they are based on inventories but are much more complex than that.

We have added “and data products” for clarification.

Pg 29604 lines 23-24. How does the fraction of  $C_{bio}$  change through the seasons? This is discussed in a later section, but you could refer to that section here, since it is an obvious question when reading this section.

We have added a reference to the later section.

Pg 29606. See my previous comment about the delta-bio for C3 vs C4 plants. How would the interpretation here change if delta-bio was strongly influenced by C4 plants?

We have added a few sentences of discussion, saying that more influence by C4 plants would raise the  $C_{ng}$  curve relative to  $C_{pet}$ , because C4 plants discriminate less strongly against the heavy isotope of carbon.

Pg 29607. Thanks for the nice discussion of the percentages from the biosphere. Does the larger fraction and larger overall magnitude of bio emissions during the cooler months imply a larger biosphere flux during the cooler months? This would be worth a few sentences of discussion.

We have added two sentences of discussion to Section 3.2. We do not try to interpret the biosphere signal here, because it is very small relative to the uncertainties.

Pg 29608 line 2. r2 should be lower case.

Changed!

Pg 29608 lines 9-14. This is hard to follow without thoroughly reading the Jiang paper. Please clarify why the semi-annual oscillation might be driven by NPP and respiration.

In the winter season, photosynthesis is largely reduced. The peak for gross primary

production is relatively flat in winter. However, there are still CO<sub>2</sub> emitted to the atmosphere by respirations from the biosphere in winter, which has a relatively sharp peak compared with the photosynthesis term. The combination of gross primary production and respiration leads to the double peaks in each year in the net ecosystem production, which contributes to the semi-annual oscillation in CO<sub>2</sub> [Jiang et al., 2012]. We have revised this in Section 3.3.

Pg 29609 lines 7-8. Why would artificial irrigation reduce the biosphere signal? Intuition would suggest an opposite effect. Please expand and reference to clarify.

We have added a comment saying that we suggest that artificial irrigation removes the seasonality that might be expected for wet versus dry seasons.

Section 3.4.1. The methodological basis for this section is not very clearly explained either in the text or the figure caption. The IMFs are sometimes referred to as “IMF 1”, “IMF 2”, etc., and sometimes by names that reflect what the IMF might represent, e.g. “annual cycle”, etc. It is not always obvious which IMF number relates to which cycle. A more detailed introduction to the method would be very helpful, perhaps in the methods section of the paper. How many IMF modes were identified? Why is the trend+IMF6 such an important curve – what is significant about IMF6 versus the other IMF modes?

The goal of this analysis is to get at the longer-term trend, which requires removing high-frequency noise and signals for which we understand the governing process. We understand the annual cycle and wish to isolate the longer-term signal. A description of the process for calculating the modes is given in Section 2.3.4. The full set of IMFs is given in Figure A3.

Pg 29610 lines 7-10. Figure 10f is the detrended signal, and is just showing the deviations from the mean, correct? It is a bit hard to follow where the 7.3 ppm standard deviation comes from when referring to this figure.

This standard deviation comes from the raw data set, since the set without the annual cycle is simply an arithmetic manipulation of the original data. Figure 10f is the sum of the final trend (only one maximum or minimum) plus IMF 6 for the data set that has had the average seasonal cycle removed. It has not had any other trend, such as linear, removed. Therefore it contains information about variations that are inter-annual.

Lines 8-13. Again, it is hard to follow how the 9.5% change is determined. Perhaps a version of figure 10f that is adjusted with a mean value matching that of the actual data and the deviations around that mean, rather than just showing the deviations from the mean would help.

We have changed the plots of the modified data set, seasonal cycle removed, to include the average of the raw data. This leads to deleting the confusing parenthetical remarks in the discussion. Thank you for pointing this out.

Lines 25-30. This is an interesting discussion about how Cff decreases might not follow economic changes perfectly, but I am not convinced that such a detailed comparison is justified by the data presented here. First, there are fairly large error bars on the Cff changes shown in figure 10f, so a decrease of 13% might be consistent with the data.



Second, the analysis makes no attempt to account for interannual variability in meteorology, which could potentially drive the observed changes.

We have deleted this discussion, since it does over interpret the data.

Pg 29611 lines 11-15. The shape of the Cff decrease appears to be different between the observations and the CARB inventory. CARB shows a minimum in 2011/2012, whereas the observations as shown in figure 10f appear to show a minimum in 2010. How can these be reconciled?

A comment has been added to address this:

There is a difference in timing between the data presented here (2010) and those from the CARB inventory (2011-2012). The difference may be due to uncertainties in the data or to the different domains covered by the two data sets.

Pg 29611, lines 23- 30 and onto the following page. Again, how would uncertainty in delta-bio influence these conclusions? A short lag between gasoline purchase and combustion makes sense, but it is hard to believe there is a 3 month lag, given that most people fill up their vehicles every week or two. What other possible explanations are there for this lag?

As mentioned above, more influence from C4 plants would raise the  $C_{ng}$  curve relative to the  $C_{pet}$  curve.

We suggest that the different domains of our data and the CARB and EIA inventories are the dominant reason for the difference in seasonality. The statement regarding lag between purchase and combustion has been deleted.

Figure 11. The presentation of this figure could be improved. The thick lines (representing the CARB inventory data) draw the eye, and give the impression that they represent some sort of smoothed average of the observational data. Yet no smoothed average of the observational data is actually given on this figure. Perhaps fits to the observational data could be added so that a more direct comparison could be made.

We have changed this figure to use the annual averages from the Pasadena data as compared with the annual CARB inventory.